ISSN 1990-7931, Russian Journal of Physical Chemistry B, 2024, Vol. 18, No. 4, pp. 1177–1198. © Pleiades Publishing, Ltd., 2024.

CHEMICAL PHYSICS OF NANOMATERIALS

Selectivity and Sensitivity Evaluation of Embedded BN-Nanostructure as a Gas Detector for Air Pollution Scavenging: a Theoretical Study

F. Mollaamin[a], *, ** and M. Monajjemi[b]

[a] *Department of Biomedical Engineering, Faculty of Engineering and Architecture, Kastamonu University, Kastamonu, Turkey*

[b] *Department of Chemical Engineering, Central Tehran Branch, Islamic Azad University, Tehran, Iran*

**e-mail: fmollaamin@kastamonu.edu.tr*

***e-mail: smollaamin@gmail.com*

Received December 5, 2023; revised April 13, 2024; accepted April 22, 2024

Abstract—This article aims to investigate the structural, electromagnetic, and thermodynamic properties of toxic gases molecules including nitric oxide (NO), nitrogen oxide (NO_2), and nitrous oxide (N_2O) during adsorption on the surface of boron nitride (B_5N_{10}) nanocage which has been decorated with aluminum (Al), carbon (C) and silicon(Si) atoms. The results denote that (NO,NO_2,N_2O) $\leftrightarrow$ (Al, C, Si)$-B_4N_{10}$ are stable complexes with the most stable adsorption site being the center of the cage ring. The partial density of states can estimate a certain charge assembly between gas molecules and (Al, C, Si)$-B_4N_{10}$ which indicates the competition among dominant complexes of metallic (Al), nonmetallic (C), metalloid/semiconductor (Si). Based on nuclear quadrupole resonance analysis, carbon-doped on B_4N_{10} has shown the lowest fluctuation in electric potential and the highest negative atomic charge including 0.1190, 0.1844, and 0.1312 coulomb in $NO \leftrightarrow C-B_4N_{10}$, NO_2 in $NO \leftrightarrow C-B_4N_{10}$, and N_2O in $NO \leftrightarrow C-B_4N_{10}$, respectively, can be an appropriate option with the highest tendency for electron accepting in the adsorption process. Furthermore, the reported results of nuclear magnetic resonance spectroscopy have exhibited that the efficiency of electron accepting for doping atoms on the (Al, C, Si)$-B_4N_{10}$ through gas molecules adsorption can be ordered as: $Si > Al \gg C$ that indicates the power of covalent bond between aluminum, carbon, silicon and these NO, NO_2, N_2O towards toxic gas removal from air. In fact, the adsorption of gas molecules can introduce spin polarization on the (Al, C, Si)$-B_4N_{10}$ which indicates that these surfaces might be applied as magnetic scavenging surface as a gas detector. Regarding infrared spectroscopy, doped nanocages of $C-B_4N_{10}$ and $Si-B_4N_{10}$ for NO, $Al-B_4N_{10}$ and $Si-B_4N_{10}$ for NO_2, $Al-B_4N_{10}$ and $C-B_4N_{10}$ for N_2O, respectively, have the most fluctuations and the highest adsorption tendency for gas molecules which can address specific questions on the individual effect of charge carriers (gas molecule-nanocage), as well as doping atoms on the overall structure. Based on the results of ΔG^{o}_{ads} amounts in this research, the maximum efficiency of Al, C, Si atoms doping of B_5N_{10} for gas molecules adsorption depends on the covalent bond between NO, NO_2, N_2O molecules and (Al, C, Si)$-B_4N_{10}$ as a potent sensor for air pollution removal.

Keywords: gas sensor, nanomaterial, boron nitride, materials modelling

DOI: 10.1134/S1990793124700507

INTRODUCTION

Boron nitride nanomaterials have been used owing to their unique characteristics such as eco-friendly attributes for pollutant adsorption, big surface area, high chemical and mechanical strength, and semiconducting property [1–4]. Boron nitride nanometerials usually exhibit semi-leading behavior, which is considered a proper alternative to carbon nanotubes [5–11]. The properties of boron and nitrogen atoms which are the first neighbors of carbon in the periodic table, make boron nitride an interesting subject of numerous studies [12–15].

In recent years, different investigations on the adsorption of chemical contaminants and applying various boron nitride nanomaterials as adsorbents for water purification have been studied [16, 17]. Various physical shapes of boron nitride (BN)-based nano adsorbents such as nanoparticles, fullerenes, nanotubes, nanofibers, nanoribbons, nanosheets, nanomeshes, nanoflowers, and hollow spheres have been broadly considered possible adsorbents owing to their exceptional characteristics such as large surface area,

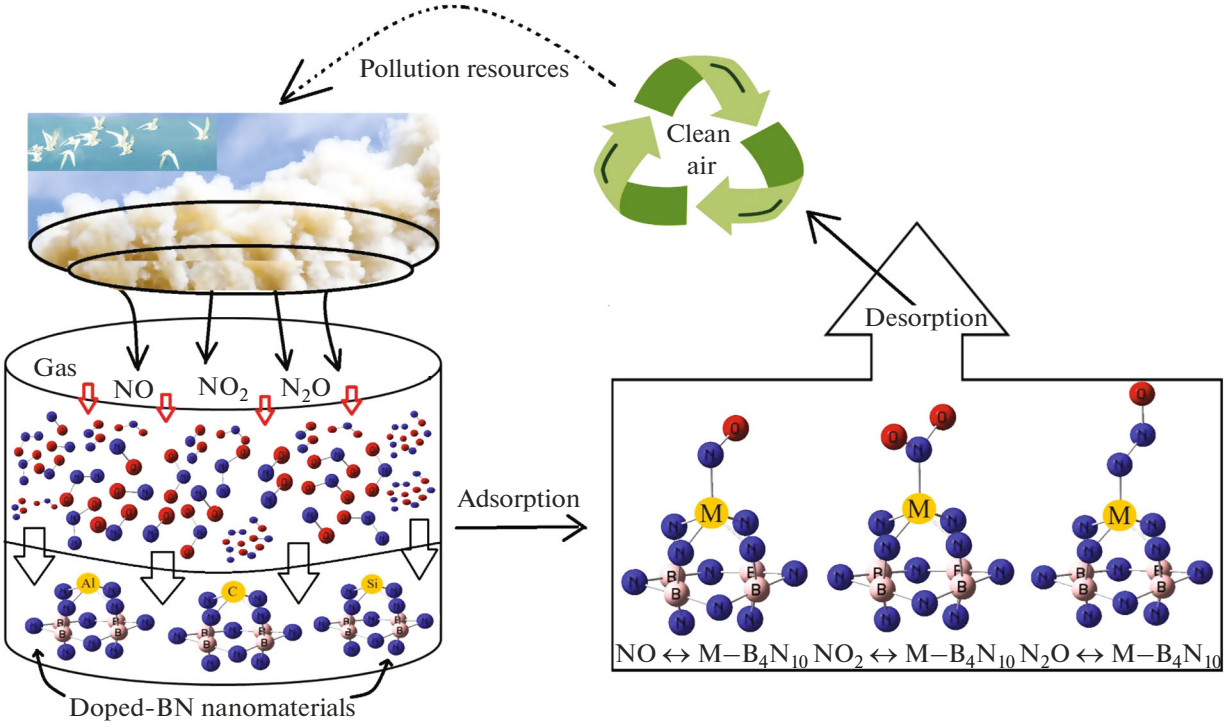

Fig. 1. Application of $M-B_4N_{10}$ towards adsorption of gas molecules of NO, NO_2, N_2O and formation of complexes: $NO \leftrightarrow Al-B_4N_{10}$, $NO \leftrightarrow C-B_4N_{10}$, $NO \leftrightarrow Si-B_4N_{10}$, $NO_2 \leftrightarrow Al-B_4N_{10}$, $NO_2 \leftrightarrow C-B_4N_{10}$, $NO_2 \leftrightarrow Si-B_4N_{10}$, $N_2O \leftrightarrow Al-B_4N_{10}$, $N_2O \leftrightarrow C-B_4N_{10}$, and $N_2O \leftrightarrow Si-B_4N_{10}$ complexes using CAM–B3LYP–D3/6-311+G(*d*, *p*), LANL2DZ calculation (M = Al, C, Si).

structural variability, great chemical/mechanical strength, abundant structural defects, high reactive sites, and functional groups [18]. Particularly, this research work aims to assess the influences of doping atoms of Al, C, Si on the B_4N_{10} for increasing gas detection through measurement of some parameters containing charge transfer, electric potential, electromagnetic and thermodynamic properties, surface area, functional group and examine the removal of selected toxic gas molecules including NO, NO_2 and N_2O during adsorption process [19].

THEORY, MATERIALS AND METHOD

Adsorption of Gas Molecules on (Al, C, Si)–B_4N_{10}

The goal of this study is to remove toxic gas molecules including NO, NO_2, N_2O from air through an eco-friendly approach by using (Al, C, Si)-doped B_4N_{10} (Fig. 1). Boron nitride nanocage was modeled in the presence of doping atoms of aluminum, carbon and silicon which can increase the gas sensing potential of BN-nanocage. In our research, sample characterization was performed by CAM–B3LYP–D3/EPR-3, LANL2DZ level of theory [20–27].

Figure 1 has shown the process adsorption of gas molecules of NO, NO_2, N_2O on the $M-B_4N_{10}$ surface which towards formation of complexes containing $NO \leftrightarrow Al-B_4N_{10}$, $NO \leftrightarrow C-B_4N_{10}$, $NO \leftrightarrow Si-B_4N_{10}$, $NO_2 \leftrightarrow Al-B_4N_{10}$, $NO_2 \leftrightarrow C-B_4N_{10}$, $NO_2 \leftrightarrow Si-B_4N_{10}$, $N_2O \leftrightarrow Al-B_4N_{10}$, $N_2O \leftrightarrow C-B_4N_{10}$, and $N_2O \leftrightarrow Si-B_4N_{10}$ by molecular modeling computations. The charge distribution of mentioned complexes is calculated due to the Bader charge analysis [28–34]. The trapping of NO, NO_2 and N_2O molecules by $M-B_4N_{10}$ (M = Al, C, Si) were successfully incorporated due to binding formation consisting of $N \rightarrow Al$, $N \rightarrow C$, $N \rightarrow Si$ (Fig. 1). Regardless of which gas molecule, the boron nitride nanocage expanded to accommodate the gas molecules by enhancing the selective sensitivity through different doping atoms of Al, C and Si (Fig. 1).

Application of Density Functional Theory Approach

Our computations have been carried out due to the conceptual of density functional theory (DFT) using the projector– augmented–wave (PAW) methodology [35–40]. The Perdew–Burke–Ernzerhof (PBE) functional under the generalized gradient approximation (GGA) was applied as the exchange-correlation functional [41–46]. The non-empirical PBE functional is recognized to relegate precise crystal specifications [47]. Commonly, where GGA functionals lose out, local

density functionals stop too. Considering the thermal conductivity compared to local density functionals, PBE does not over attach structures, and therefore the interatomic force constants are not too flexible. All in all, the lattice thermal conductivity is entirely the same whether using local density or GGA functionals [48].

Hohenberg–Kohn (HK) functions have rigidly made the electronic density permissible as fundamental variable to electronic and structure computations. In other words, development of the applied DFT methodology only became notable after Kohn W. and Sham L.J. released their reputable series of equations which are introduced as Kohn–Sham (KS) equations [49, 50]. Considering the electronic density within the KS image directs us to a remarkable reduction of quantum computing. Thus, the KS methodology lightens the route for pursuing systems that cannot be discussed by conventional ab-initio methodologies. Kohn and Sham" introduces the solution which brings up the mono-electronic orbitals to account the kinetic energy in a simple and relatively exact, by finding a residual modification that might be computed apart [51]. Therefore, the precise exchange energy functional is described by the Kohn–Sham orbitals in lieu of the density which is cited as the indirect density functional. This research has employed the penetration of the hybrid functional of three-parameter basis set of B3LYP within the conception of DFT upon theoretical computations [52–61].

In this article, the rigid PES using DFT calculations have been accomplished by using Gaussian 16 revision C.01 program package [62]. The input Z-matrix for adsorption of NO, NO_2 and N_2O molecules in air by the M–B_4N_{10} has been provided with GaussView 6.1 [63] due to the rigid system and coordination format of which a blank line has been cited and using 6-311+G(d, p), EPR-3, LANL2DZ basis set to distinguish chemical shielding, frequencies, thermodynamic properties, electrostatic and electronic potential, natural atomic charges, projected density of state and other quantum properties for this work. In this study, the interaction between gas molecules and M–B_4N_{10} was modeled and analyzed. As revealed by DFT-based analysis, the potency of M–B_4N_{10} for grabbing gas molecules was determined mainly by the electronegativity of the functional groups, as well as the interaction between the M–B_4N_{10} and the gas molecules.

RESULTS AND DISCUSSION

Gas molecules that are dominant pollution in air are NO, NO_2 and N_2O. The data has evaluated the efficiency of boron nitride nanocage doped with aluminum, carbon, silicon (M–B_4N_{10}) for gas detection. In fact, it can be remarked the chemisorptive nature of the bond among the gas molecules with boron and nitrogen elements through the equilibrium distribution of doping atoms, B_5N_{10}, and a monolayer attribute.

Projected Density of State and Electronic Evaluating

The electronic structures of gas adsorption (G=NO, NO_2, N_2O) using M (M = Al, C, Si)-doped B_5N_{10} as the selective sensor [64, 65] for detecting and grabbing gas molecules in the air have been investigated to simplify subsequent study for interfacial electronic properties using CAM–B3LYP–D3/6-311+G(*d*, *p*), LANL2DZ level of theory. Figure 2 show the projected density of state (PDOS) of M ↔ (Al, C, Si)–B_4N_{10} through gas molecules adsorption. The appearance of the energy states (*p*-orbital) of Al, C, Si, N, O within the gap of (Al, C, Si)–B_4N_{10} induces the reactivity of the system. It is clear from the figure that after trapping with gas molecules, there is a significant contribution of *p*-orbital in the unoccupied level. Therefore, the curve of partial PDOS has described that the *p* states of N atoms in gas molecules and Al, C, Si atoms in M–B_4N_{10} are overcoming due to the conduction band (Fig. 2). A distinguished adsorption trait might be seen in G ↔ M–B_4N_{10} because of the potent interaction between the *p* states of nitrogen atom in gas molecules with *p* states of Al, C, Si in M–B_4N_{10} complexes near the Fermi energy. Furthermore, the essence of covalent traits for these clusters has displayed the similar energy value and image of the PDOS for the *p* states of N, O and Al, C, Si through gas toxic removal from air (Fig. 2).

Figure 2 shows that NO ↔ Al–B_4N_{10}, NO ↔ Si–B_4N_{10}, NO_2 ↔ C–B_4N_{10}, NO_2 ↔ Si–B_4N_{10}, N_2O ↔ Al–B_4N_{10}, and N_2O ↔ Si–B_4N_{10} complexes through gas molecules adsorption, respectively, have the most contribution at the middle of the conduction band between –5 to –10 eV, while contribution of boron and nitrogen states are enlarged and similar together, and adsorbing of NO, NO_2, N_2O depicts interfacial electronic of the B_5N_{10} for selection of these cations. NO ↔ Al–B_4N_{10} has indicated one sharp peak for Al in Fig. 2a, while NO ↔ Si–B_4N_{10} (Fig. 2b) has exhibited one sharp peak around –7.5 eV for Si atom. Furthermore, NO_2 ↔ C–B_4N_{10} (Fig. 2c) and NO_2 ↔ Si–B_4N_{10} (Fig. 2d) complexes, respectively, have exhibited a strong peak around –9 eV through the graphs for C atom and –7.5 eV for Si atom. Furthermore, the Al graph with a sharp peak around –9 eV in N_2O ↔ Al–B_4N_{10} (Fig. 2e) and Si graph in N_2O ↔ Si–B_4N_{10} (Fig. 2f) with a sharp peak around –7.5 eV, respectively, have been shown. Therefore, the order potency of gas adsorption by doping atoms of Al, C, Si on M–B_4N_{10} based on the PDOS might be shifted as: Si–B_4N_{10} > Al–B_4N_{10} ⩾ C–B_4N_{10}. The partial density of states or PDOS can also estimate a certain charge assembly between NO, NO_2, N_2O and M–B_4N_{10} through gas molecules adsorption. On the other hand, the above data can illustrate that the complex dominant of metallic (Al), nonmetallic (C), metalloid/semiconductor (Si) and an exact degree of covalent

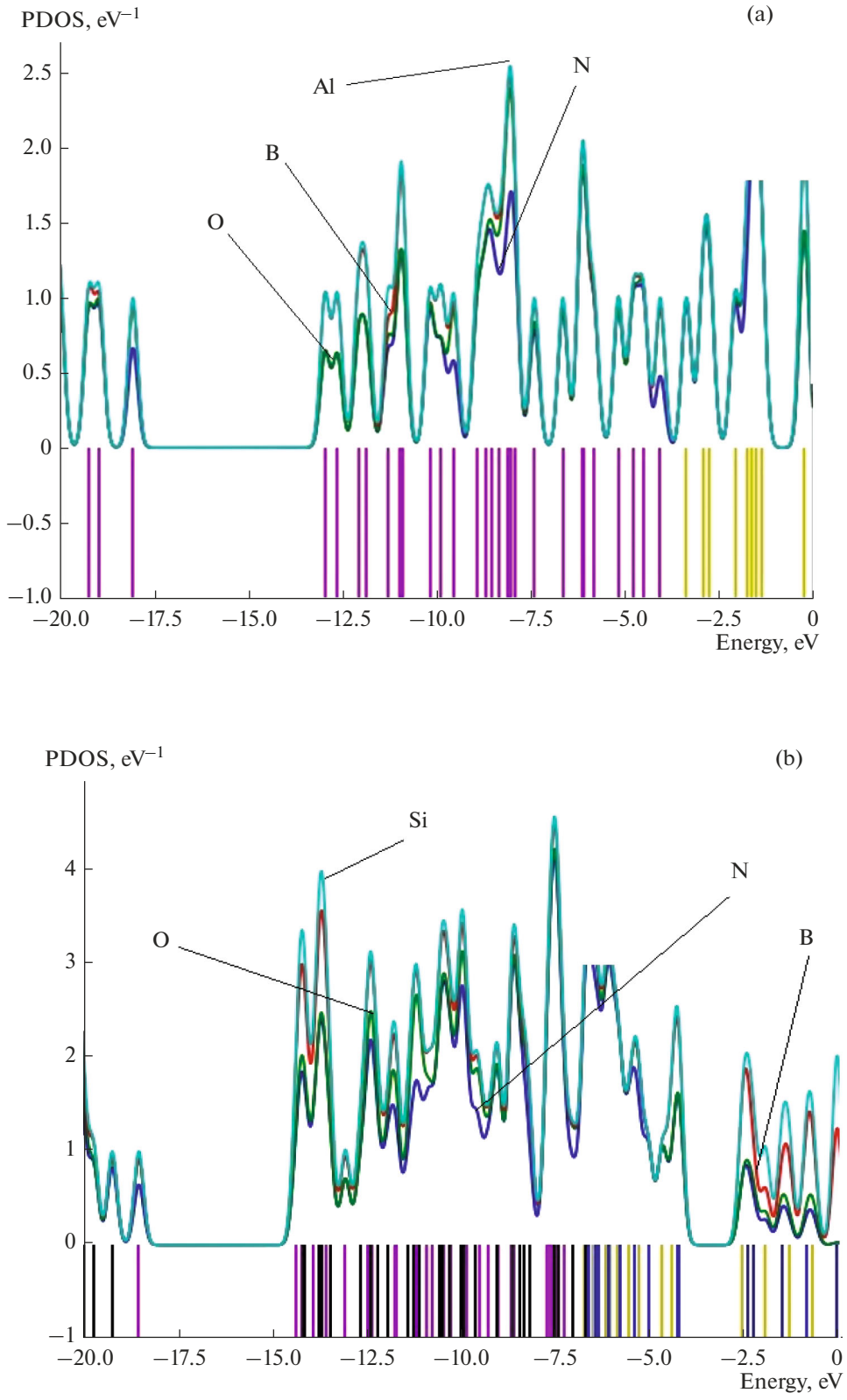

Fig. 2. PDOS of gas molecules of NO, NO_2, N_2O adsorbed on $M-B_4N_{10}$ including (a) NO ↔ $Al-B_4N_1$, (b) NO ↔ $Si-B_4N_{10}$, (c) NO_2 ↔ $C-B_4N_{10}$, (d) NO_2 ↔ $Si-B_4N_{10}$, (e) N_2O ↔ $Al-B_4N_{10}$, and (f) N_2O ↔ $Si-B_4N_{10}$ complexes by CAM–B3LYP–D3/6-311+G(*d*, *p*), LANL2DZ.

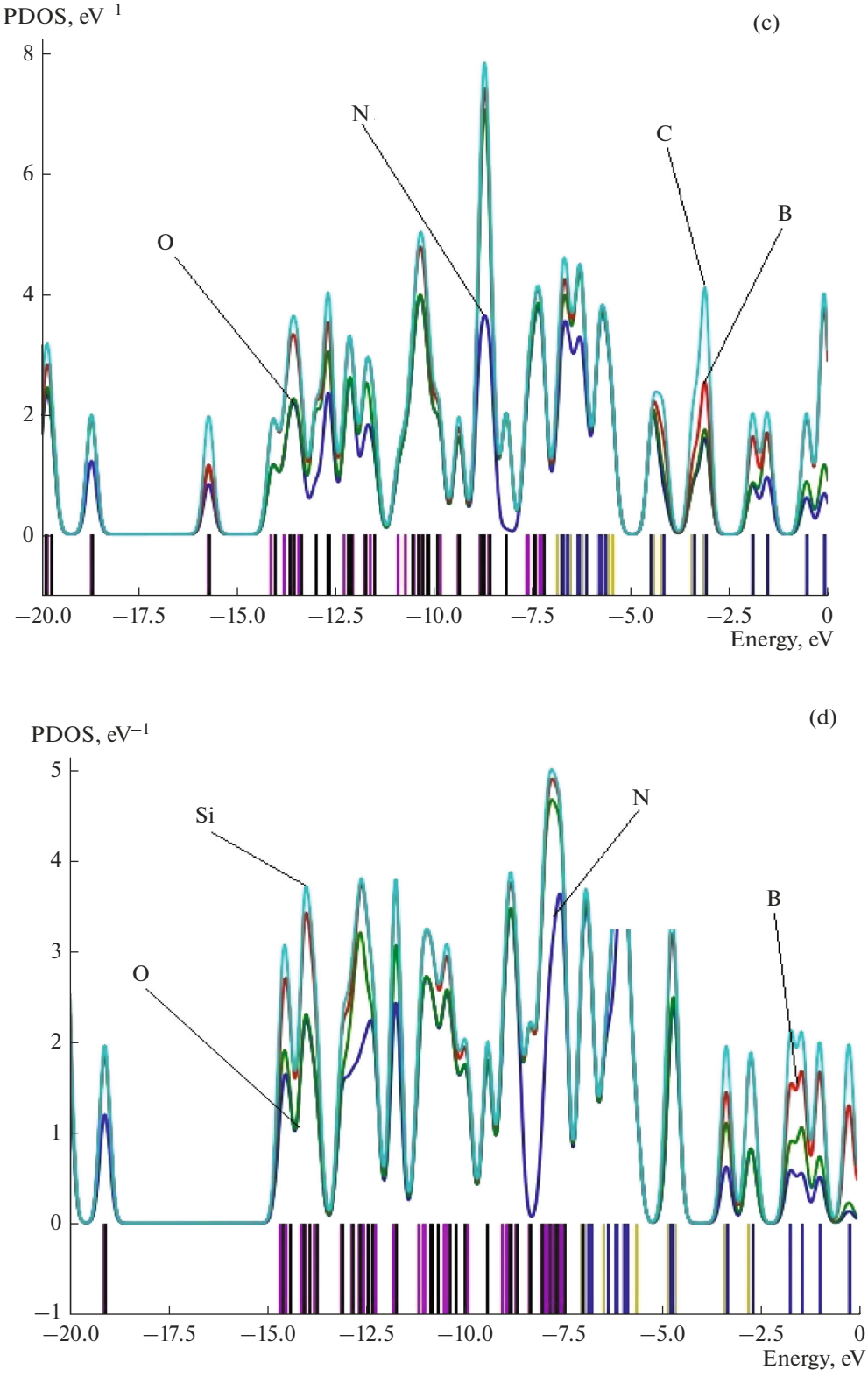
PDOS, eV^{-1}
(c)
8
6
4
2
0
N
C
B
O
−20.0
−17.5
−15.0
−12.5
−10.0
−7.5
−5.0
−2.5
0
Energy, eV
(d)
PDOS, eV^{-1}
5
4
3
2
1
0
−1
Si
N
B
O
−20.0
−17.5
−15.0
−12.5
−10.0
−7.5
−5.0
−2.5
0
Energy, eV

Fig. 2. (Contd.)

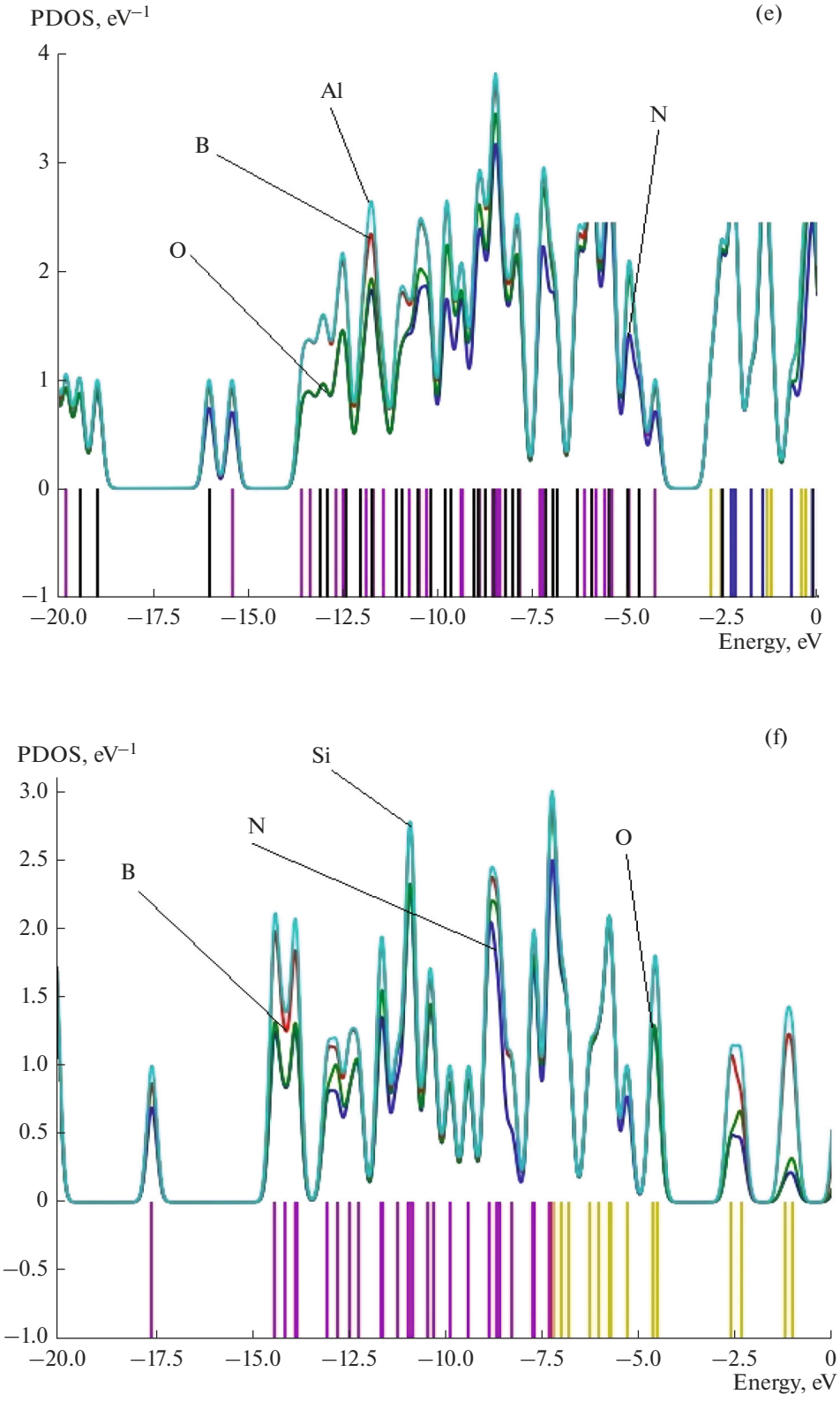

Fig. 2. (Contd.)

traits can describe the augmenting of the stability of M–B_4N_{10} during the process of ion adsorption (Fig. 2).

Insight to Nuclear Quadrupole Resonance

In this research, the calculated nuclear quadrupole resonance (NQR) specifications extracted from electrostatic properties have been calculated for the trapping of toxic gas molecules of NO, NO_2, N_2O in the M–B_4N_{10} which is accord to the results of the nuclear quadrupole moment, a trait of the nucleus, and the electric field gradient (EFG) in the neighborhood of the nucleus. As the EFG at the citation of the nucleus in NO, NO_2, N_2O is allocated by the valence electrons twisted in the particular attachment with close nuclei of M–B_4N_{10} through trapping of gas molecules, the NQR frequency at which transitions occur is particular for G ↔ M–B_4N_{10} complexes (G = NO, NO_2, N_2O) (Table 1).

Nuclear quadrupole resonance is a straight frame of the interaction of the quadrupole moment with the EFG which is produced by the electronic structure of its ambiance. Therefore, the NQR transition frequencies are symmetric to the electric quadrupole moment of the nucleus and a measurement of the strength of the local EFG [66–69]. The electric potential as the quantity of work energy through carrying over the electric charge from one position to another position in the essence of electric field has been evaluated for NO ↔ Al–B_4N_{10}, NO ↔ C–B_4N_{10}, NO ↔ Si–B_4N_{10}, NO_2 ↔ Al–B_4N_{10}, NO_2 ↔ C–B_4N_{10}, NO_2 ↔ Si–B_4N_{10}, N_2O ↔ Al–B_4N_{10}, N_2O ↔ C–B_4N_{10}, and N_2O ↔ Si–B_4N_{10} complexes using CAM–B3LYP–D3/EPR-3, LANL2DZ level of theory (Table 1). In Table 1, the Bader charge and electronic potential properties of Al, C, Si–B, N in M–B_4N_{10} and N, O of gas molecules trapped on doped-boron nitride nanocages have been investigated. The amounts indicate that with increasing the negative charge of different atoms, the electric potential resulted from NQR calculations increase. Moreover, the doping atoms of Al(15), C(15), Si(15) on the B_4N_{10} have shown the most potential for accepting the electron from electron donor of N(1) in NO, NO_2, N_2O adsorbed on the B_4N_{10} (Table 1).

Furthermore, in Fig. 3, it has been sketched the electric potential of nuclear quadrupole resonance for some atoms of Al, C, Si/B, N in M–B_4N_{10} and N, O of gas molecules trapped on doped-boron nitride nanocages which has been calculated by CAM–B3LYP–D3/EPR-3, LANL2DZ. In Fig. 3a and 3b it was observed the behavior of NO adsorption on the Al–B_4N_{10} and NO ↔ Si–B_4N_{10}, respectively, with high sensitivity based on relation coefficient of R^2 = 0.9945 and R^2 = 0.9827. Adsorption of NO_2 on the C–B_4N_{10} and Si–B_4N_{10} in Figs. 3c and 3d, respectively, has illustrated the analogous with the highest sensing of R^2 = 0.9925 and R^2 = 0.9743. In addition, Figs. 3e and 3f has resulted that N_2O ↔ Al–B_4N_{10}, and N_2O ↔ Si–B_4N_{10}, respectively, has a good detecting for N_2O removal from air through relation coefficient of R^2 = 0.9637 and R^2 = 0.9006.

It's vivid that the curve of M–B_4N_{10} is waved by these gas molecules. The fluctuated peaks for electric potential have been shown around NO_2 > NO > N_2O trapping on the M–B_4N_{10} which present the electron accepting characteristics of nitrogen and oxygen versus the aluminum, carbon and silicon doped on the B_5N_{10} (Fig. 3). Besides, it can be considered that silicon as a semiconductor element in the functionalized B_5N_{10} might have more impressive sensitivity for accepting the electrons from NO (Fig. 3b), NO_2 (Fig. 3d) and N_2O (Fig. 3f) in the process of adsorption mechanism. However, carbon-doped on B_5N_{10} has shown the lowest fluctuation between Bader charge versus electric potential extract from NQR parameters and the highest negative atomic charge including 0.1190 coulomb in NO ↔ C–B_4N_{10}, 0.1844 coulomb in NO_2 ↔ C–B_4N_{10}, and 0.1312 coulomb in N_2O ↔ C–B_4N_{10} which can be an appropriate option with the highest tendency for electron accepting in the adsorption current (Table 1). Aluminum and silicon doped on B_5N_{10} (adsorbents) with an average of 1.1 coulomb of atomic charge on (Al, Si)–B_4N_{10} have shown similar behavior in the procedure of gas molecules (adsorbates) removal. In fact, the uptake of gas molecules has been known to be associated with M–B_4N_{10}, indicating that the adsorbed gas molecules in the M–doped nanocage can be internalized through a different pathway from pristine nanocage.

Analysis of Nuclear Magnetic Resonance Spectra

Based on resulted amounts, nuclear magnetic resonance (NMR) spectra of M–B_4N_{10} (M = Al, C, Si) as the potent sensor for adsorbing toxic gas molecules containing NO, NO_2, N_2O molecules can unravel the efficiency of M–B_4N_{10} for detecting and removing of these hazardous gases in air as an ecofriendly approach.

From the DFT calculations, it has been attained the chemical shielding (CS) tensors in the principal axes system to estimate the isotropic chemical-shielding (CSI) and anisotropic chemical-shielding (CSA) [70]:

$$\sigma_{iso} = \frac{\sigma_{11} + \sigma_{22} + \sigma_{33}}{3}, \quad (1)$$

$$\sigma_{aniso} = \sigma_{33} - (\sigma_{22} + \sigma_{11})/2. \quad (2)$$

Table 1. The electric potential (E_p/a.u.) and Bader charge (Q/coulomb) through NQR calculation for NO ↔ Al–B_4N_{10}, NO ↔ C–B_4N_{10}, NO ↔ Si–B_4N_{10}, NO_2 ↔ Al–B_4N_{10}, NO_2 ↔ C–B_4N_{10}, NO_2 ↔ Si–B_4N_{10}, N_2O ↔ Al–B_4N_{10}, N_2O ↔ C–B_4N_{10}, and N_2O ↔ Si–B_4N_{10} complexes using CAM–B3LYP–D3/EPR-3, LANL2DZ calculation

NO ↔ Al–B_4N_{10}			NO ↔ C–B_4N_{10}			NO ↔ Si–B_4N_{10}		
atom	Q	E_p	atom	Q	E_p	atom	Q	E_p
N(1)	−0.18	−18.08	N(1)	0.14	−18.18	N(1)	−0.19	−18.25
O(2)	−0.02	−21.93	O(2)	−0.09	−22.20	O(2)	−0.08	−22.21
B(3)	0.30	−11.23	B(3)	0.03	−11.28	B(3)	0.02	−11.28
N(4)	−0.17	−18.09	N(4)	−0.01	−18.29	N(4)	0.01	−18.28
N(5)	−0.15	−18.05	N(5)	−0.04	−18.27	N(5)	0.00	−18.26
B(6)	0.30	−11.23	B(6)	0.03	−11.28	B(6)	0.03	−11.28
B(7)	0.29	−11.22	B(7)	0.03	−11.28	B(7)	0.03	−11.28
B(8)	0.29	−11.23	B(8)	0.03	−11.28	B(8)	0.03	−11.28
N(9)	−0.15	−18.06	N(9)	−0.02	−18.28	N(9)	−0.02	−18.27
N(10)	−0.14	−18.04	N(10)	−0.04	−18.27	N(10)	0.00	−18.26
N(11)	−0.26	−18.11	N(11)	−0.03	−18.26	N(11)	−0.24	−18.28
N(12)	−0.25	−18.11	N(12)	−0.03	−18.26	N(12)	−0.23	−18.28
N(13)	−0.25	−18.11	N(13)	−0.03	−18.26	N(13)	−0.23	−18.28
N(14)	−0.26	−18.11	N(14)	−0.03	−18.26	N(14)	−0.23	−18.28
Al(15)	1.00	−43.64	C(15)	0.12	−14.54	Si(15)	1.10	−1.759
N(16)	−0.16	−18.06	N(16)	−0.02	−18.28	N(16)	−0.02	−18.27
N(17)	−0.17	−18.09	N(17)	−0.01	−18.29	N(17)	0.01	−18.28
NO_2 ↔ Al–B_4N_{10}			NO_2 ↔ C–B_4N_{10}			NO_2 ↔ Si–B_4N_{10}		
atom	Q	E_p	atom	Q	E_p	atom	Q	E_p
N(1)	−0.13	−18.18	N(1)	0.161	−18.11	N(1)	−0.11	−18.14
O(2)	−0.18	−22.26	O(2)	−0.11	−22.22	O(2)	−0.13	−22.24
B(3)	0.09	−11.25	B(3)	0.03	−11.28	B(3)	0.03	−11.27
N(4)	0.00	−18.25	N(4)	−0.01	−18.28	N(4)	0.01	−18.27
N(5)	−0.03	−18.22	N(5)	−0.04	−18.26	N(5)	−0.00	−18.25
B(6)	0.10	−11.25	B(6)	0.03	−11.28	B(6)	0.03	−11.27
B(7)	0.09	−11.25	B(7)	0.03	−11.28	B(7)	0.03	−11.27
B(8)	0.10	−11.25	B(8)	0.03	−11.28	B(8)	0.03	−11.27
N(9)	−0.03	−18.23	N(9)	−0.02	−18.27	N(9)	−0.01	−18.26
N(10)	−0.03	−18.22	N(10)	−0.04	−18.26	N(10)	−0.00	−18.25
N(11)	−0.26	−18.25	N(11)	−0.03	−18.25	N(11)	−0.22	−18.27
N(12)	−0.27	−18.25	N(12)	−0.03	−18.25	N(12)	−0.23	−18.27
N(13)	−0.26	−18.25	N(13)	−0.03	−18.25	N(13)	−0.22	−18.27
N(14)	−0.27	−18.25	N(14)	−0.03	−18.25	N(14)	−0.23	−18.27
Al(15)	1.31	−1.11	C(15)	0.18	−14.51	Si(15)	1.16	−1.74
N(16)	−0.03	−18.23	N(16)	−0.02	−18.27	N(16)	−0.01	−18.26
N(17)	0.00	−18.25	N(17)	−0.01	−18.28	N(17)	0.01	−18.27

Table 1. (Contd.)

$NO \leftrightarrow Al{-}B_4N_{10}$			$NO \leftrightarrow C{-}B_4N_{10}$			$NO \leftrightarrow Si{-}B_4N_{10}$		
O(18)	−0.18	−22.26	O(18)	−0.11	−22.22	O(18)	−0.13	−22.24
$N_2O \leftrightarrow Al{-}B_4N_{10}\_NC$			$N_2O \leftrightarrow C{-}B_4N_{10}\_NC$			$N_2O \leftrightarrow Si{-}B_4N_{10}\_NC$		
atom	Q	E_p	atom	Q	E_p	atom	Q	E_p
N(1)	−0.29	−18.14	N(1)	0.024	−18.23	N(1)	−0.25	−18.25
N(2)	−0.03	−18.02	N(2)	0.07	−18.19	N(2)	0.10	−18.18
B(3)	0.30	−11.22	B(3)	0.02	−11.27	B(3)	0.02	−11.27
N(4)	−0.16	−18.06	N(4)	−0.01	−18.27	N(4)	−0.01	−18.26
N(5)	−0.13	−18.04	N(5)	−0.04	−18.26	N(5)	−0.01	−18.26
B(6)	0.30	−11.22	B(6)	0.03	−11.28	B(6)	0.03	−11.27
B(7)	0.30	−11.23	B(7)	0.03	−11.28	B(7)	0.03	−11.27
B(8)	0.30	−11.22	B(8)	0.03	−11.28	B(8)	0.03	−11.27
N(9)	−0.167	−18.08	N(9)	−0.00	−18.28	N(9)	0.01	−18.28
N(10)	−0.13	−18.04	N(10)	−0.05	−18.26	N(10)	−0.01	−18.26
N(11)	−0.26	−18.10	N(11)	−0.02	−18.25	N(11)	−0.24	−18.27
N(12)	−0.26	−18.10	N(12)	−0.02	−18.25	N(12)	−0.23	−18.27
N(13)	−0.25	−18.10	N(13)	−0.03	−18.25	N(13)	−0.23	−18.27
N(14)	−0.26	−18.10	N(14)	−0.02	−18.25	N(14)	−0.23	−18.27
Al(15)	1.07	−43.64	C(15)	0.13	−14.51	Si(15)	1.12	−1.75
N(16)	−0.17	−18.10	N(16)	−0.00	−18.28	N(16)	0.01	−18.28
N(17)	−0.16	−18.06	N(17)	−0.01	−18.27	N(17)	−0.00	−18.26
O(18)	0.00	−21.94	O(18)	−0.13	−22.23	O(18)	−0.12	−22.23

The chemical shielding extracts from NMR can be applied for allocating the structural and geometrical specifications of materials [71–74].

As a matter of fact, gauge invariant atomic orbital (GIAO) methodology has been recommended as a valid methodology for NMR parameter computations and Our own N-layered Integrated molecular orbital and molecular mechanics (ONIOM) has caught many regards for gaining NMR chemical shielding of gas molecule-surface complexes such as isotropic chemical shielding appears in Eq. (3):

$$\sigma_{\text{iso, ONIOM}} = \sigma_{\text{iso, high(QM1)}} + \sigma_{\text{iso, medium(QM2)}} + \sigma_{\text{iso, low(QM3)}}. \quad (3)$$

The NMR data of isotropic (σ_{iso}) and anisotropic shielding tensors (σ_{aniso}) of gas molecules trapped in the $M{-}B_4N_{10}$ towards formation of $NO \leftrightarrow Al{-}B_4N_{10}$, $NO \leftrightarrow C{-}B_4N_{10}$, $NO \leftrightarrow Si{-}B_4N_{10}$, $NO_2 \leftrightarrow Al{-}B_4N_{10}$, $NO_2 \leftrightarrow C{-}B_4N_{10}$, $NO_2 \leftrightarrow Si{-}B_4N_{10}$, $N_2O \leftrightarrow Al{-}B_4N_{10}$, $N_2O \leftrightarrow C{-}B_4N_{10}$, and $N_2O \leftrightarrow Si{-}B_4N_{10}$ complexes have been computed by Gaussian 16 revision C.01 program package [62] and been shown in Table 2.

In Table 2, NMR data has reported the notable amounts for NO, NO_2, N_2O which were adsorbed on the $M{-}B_4N_{10}$ as the selective sensor for detecting gas molecules in air. The observed increase in the chemical shift anisotropy spans for N atoms, O(2) for NO/N_2O adsorption and O(2)/O(18) for NO_2 adsorption on the $M{-}B_4N_{10}$. The observed weak signal intensity near the parallel edge of the nanocage pattern may be due to boron binding induced non-spherical distribution of these complexes.

It is remarkable that doping of Al, C, Si on B_5N_{10} might promote the stability of nanocage that results in enhanced magnetic alignment of complexes. Interestingly, the reported results show that Al, C, Si elements can be optimized to achieve optimal alignment of nanocage in the presence of an applied magnetic field.

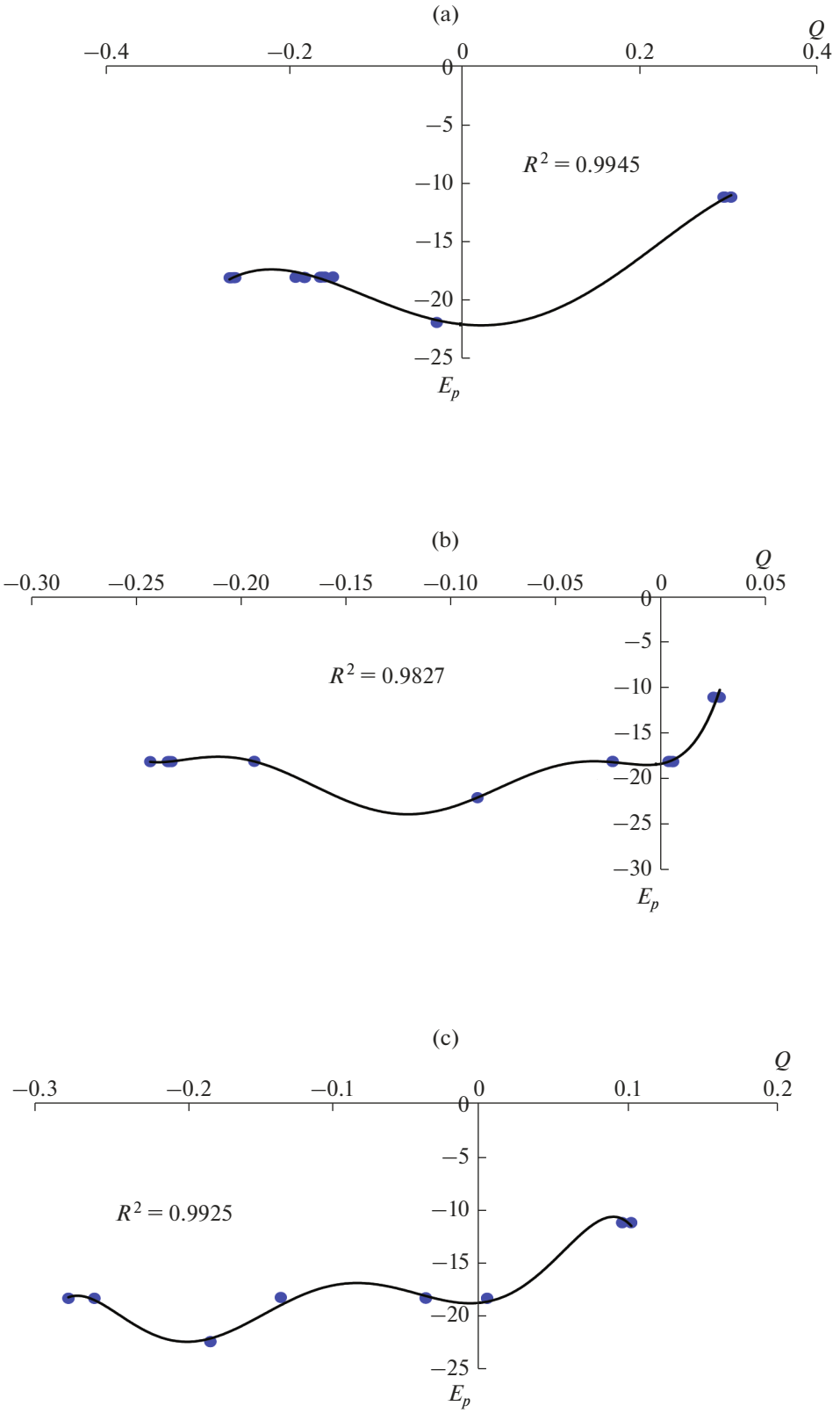

Fig. 3. Electric potential (E_p/a.u.) versus Bader charge (Q/coulomb) through NQR calculation for (a) NO ↔ Al–B_4N_{10}, (b) NO ↔ Si–B_4N_{10}, (c) NO_2 ↔ C–B_4N_{10}, (d) NO_2 ↔ Si–B_4N_{10}, (e) N_2O ↔ Al–B_4N_{10}, and (f) N_2O ↔ Si–B_4N_{10} complexes by CAM–B3LYP–D3/EPR-3, LANL2DZ.

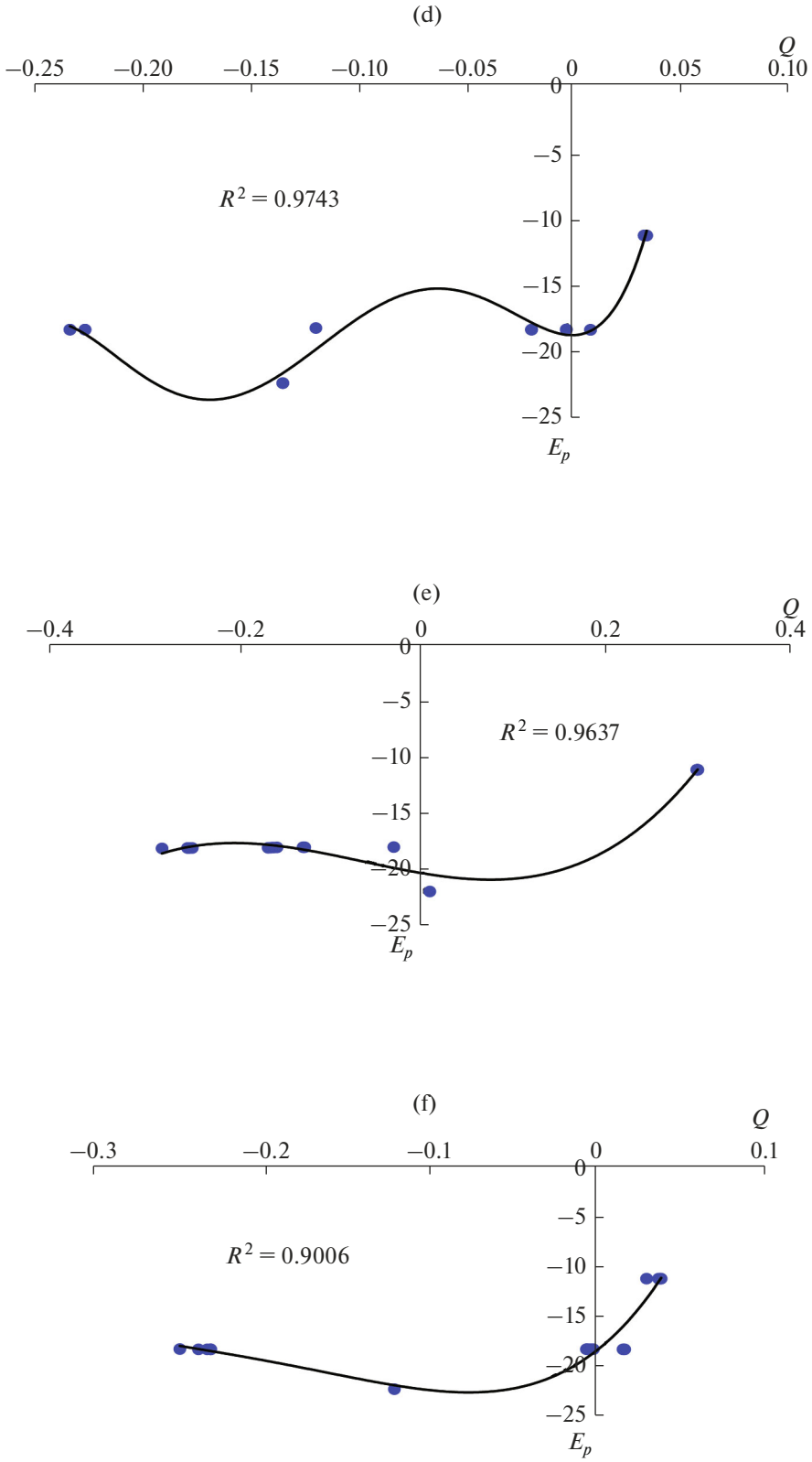
(d)
Q
−0.25 −0.20 −0.15 −0.10 −0.05 0 0.05 0.10
0
−5
−10
−15
−20
−25
$R^2 = 0.9743$
E_p
(e)
Q
−0.4 −0.2 0 0.2 0.4
0
−5
−10
−15
−20
−25
$R^2 = 0.9637$
E_p
(f)
Q
−0.3 −0.2 −0.1 0 0.1
0
−5
−10
−15
−20
−25
$R^2 = 0.9006$
E_p

Fig. 3. (Contd.)

Table 2. Data of NMR shielding tensors for selected atoms of NO ↔ Al–B_4N_{10}, NO ↔ C–B_4N_{10}, NO ↔ Si–B_4N_{10}, NO_2 ↔ Al–B_4N_{10}, NO_2 ↔ C–B_4N_{10}, NO_2 ↔ Si–B_4N_{10}, N_2O ↔ Al–B_4N_{10}, N_2O ↔ C–B_4N_{10}–NC, and N_2O ↔ Si–B_4N_1 complexes using CAM–B3LYP–D3/6-311+G(*d*, *p*), LANL2DZ calculation

NO ↔ Al–B_4N_{10}			NO ↔ C–B_4N_{10}			NO ↔ Si–B_4N_{10}		
atom	σ_{iso}	σ_{aniso}	atom	σ_{iso}	σ_{aniso}	atom	σ_{iso}	σ_{aniso}
N(1)	8623.32	27621.57	N(1)	767.22	574.98	N(1)	192.56	384.90
O(2)	19114.01	60055.67	O(2)	1697.96	1904.72	O(2)	483.66	446.82
B(3)	86.22	111.56	B(3)	83.21	75.50	B(3)	82.97	83.28
N(4)	398.76	5613.57	N(4)	698.49	846.36	N(4)	632.16	715.69
N(5)	1776.02	4560.20	N(5)	419.17	284.09	N(5)	460.89	248.70
B(6)	49.90	132.42	B(6)	84.90	76.89	B(6)	82.84	84.06
B(7)	88.70	112.26	B(7)	83.80	78.10	B(7)	83.55	82.75
B(8)	71.25	98.23	B(8)	84.84	75.04	B(8)	82.66	83.30
N(9)	673.90	3914.01	N(9)	421.55	778.5	N(9)	336.67	513.56
N(10)	2101.53	4479.16	N(10)	417.63	182.60	N(10)	457.73	296.56
N(11)	1145.30	6048.66	N(11)	574.52	402.81	N(11)	461.37	425.06
N(12)	284.26	4440.80	N(12)	538.46	433.46	N(12)	468.95	388.36
N(13)	434.51	1761.12	N(13)	581.63	365.00	N(13)	499.78	451.39
N(14)	681.36	2664.93	N(14)	556.56	519.43	N(14)	465.66	387.06
Al(15)	44.57	1469.07	C(15)	8.39	43.65	Si(15)	14.62	12.52
N(16)	496.25	2696.81	N(16)	390.13	810.91	N(16)	329.86	536.87
N(17)	2319.99	5536.37	N(17)	685.03	860.42	N(17)	611.84	711.69
NO_2 ↔ Al–B_4N_{10}			NO_2 ↔ C–B_4N_{10}			NO_2 ↔ Si–B_4N_{10}		
atom	σ_{iso}	σ_{aniso}	atom	σ_{iso}	σ_{aniso}	atom	σ_{iso}	σ_{aniso}
N(1)	127.48	408.57	N(1)	355.92	240.70	N(1)	351.76	362.40
O(2)	736.54	2843.97	O(2)	1494.82	344.94	O(2)	1640.67	1363.15
B(3)	72.81	102.90	B(3)	82.62	80.50	B(3)	86.75	83.11
N(4)	1345.89	3740.25	N(4)	675.11	728.24	N(4)	667.28	729.72
N(5)	1403.66	2050.89	N(5)	419.86	100.44	N(5)	449.04	212.10
B(6)	70.81	100.78	B(6)	83.98	77.82	B(6)	87.42	81.72
B(7)	72.85	102.84	B(7)	82.60	80.57	B(7)	86.74	83.16
B(8)	70.79	100.83	B(8)	83.99	77.83	B(8)	87.42	81.75
N(9)	593.07	1535.08	N(9)	337.76	725.45	N(9)	313.33	635.74
N(10)	1405.28	2053.34	N(10)	419.80	100.64	N(10)	448.95	211.72
N(11)	43.11	2097.30	N(11)	565.20	477.6	N(11)	444.08	395.29
N(12)	69.38	1911.86	N(12)	585.31	503.19	N(12)	449.18	406.40
N(13)	44.49	2099.87	N(13)	565.92	478.21	N(13)	444.94	395.52
N(14)	68.31	1917.77	N(14)	585.41	503.81	N(14)	449.40	407.20
Al(15)	581.14	354.23	C(15)	49.99	87.76	Si(15)	13.41	10.65
N(16)	593.69	1538.86	N(16)	337.34	725.90	N(16)	313.06	636.08

Table 2. (Contd.)

$NO \leftrightarrow Al{-}B_4N_{10}$			$NO \leftrightarrow C{-}B_4N_{10}$			$NO \leftrightarrow Si{-}B_4N_{10}$		
N(17)	1340.04	3734.09	N(17)	674.45	727.66	N(17)	666.68	729.12
O(18)	732.81	2835.74	O(18)	1494.73	344.88	O(18)	1640.63	1363.26
$N_2O \leftrightarrow Al{-}B_4N_{10}$			$N_2O \leftrightarrow C{-}B_4N_1$			$N_2O \leftrightarrow Si{-}B_4N_{10}$		
atom	σ_{iso}	σ_{aniso}	atom	σ_{iso}	σ_{aniso}	atom	σ_{iso}	σ_{aniso}
N(1)	267.89	453.18	N(1)	41.33	1687.67	N(1)	78.93	567.22
N(2)	168.13	170.90	N(2)	864.66	932.50	N(2)	625.27	512.88
B(3)	99.01	75.58	B(3)	69.95	136.15	B(3)	76.10	120.90
N(4)	0.05	389.96	N(4)	1952.94	3217.63	N(4)	1209.22	2081.44
N(5)	14.97	299.65	N(5)	4341.51	5912.65	N(5)	2524.64	3080.04
B(6)	95.88	75.63	B(6)	70.45	117.46	B(6)	84.99	95.13
B(7)	95.20	76.47	B(7)	97.47	105.05	B(7)	89.80	100.23
B(8)	98.22	75.7	B(8)	86.46	108.18	B(8)	88.32	97.13
N(9)	102.43	331.31	N(9)	747.56	7237.79	N(9)	278.88	3989.46
N(10)	29.83	283.75	N(10)	2423.12	3261.16	N(10)	1756.26	2124.54
N(11)	467.03	400.15	N(11)	381.13	2220.66	N(11)	220.22	1341.21
N(12)	501.16	490.33	N(12)	423.86	1511.34	N(12)	309.98	1116.88
N(13)	470.79	469.84	N(13)	98.49	2976.83	N(13)	361.77	1430.73
N(14)	441.85	357.38	N(14)	71.03	2659.88	N(14)	265.39	1247.17
Al(15)	563.07	31.28	C(15)	6.56	79.12	Si(15)	28.77	17.21
N(16)	406.24	655.66	N(16)	1026.01	6313.65	N(16)	539.06	3707.21
N(17)	149.96	150.11	N(17)	2268.01	3633.97	N(17)	1376.43	2295.01
O(18)	748.70	361.86	O(18)	2712.98	4012.29	O(18)	1803.07	1337.35

In fact, the adsorption of NO, NO_2, N_2O can introduce spin polarization on the $M{-}B_4N_{10}$ which indicates that these surfaces might be applied as magnetic scavenging surface as a gas detector. In fact, it is revealed that the isotropic and anisotropic shielding fluctuate with the occupancy in the electron accepting gas molecules trapped in the atom-doped on the boron nitride nanocage. Figure 4 exhibited the same tendency of shielding for boron and nitrogen; however, a considerable deviation exists from doping atoms of Al(15), C(15) and Si(15) through interaction with N(1) of NO, NO_2, N_2O during adsorbing on the B_5N_{10}.

In Fig. 4, gas molecules of NO, NO_2, N_2O in the complexes of $NO \leftrightarrow C{-}B_4N_{10}$ (Fig. 4a), $NO \leftrightarrow Si{-}B_4N_{10}$ (Fig. 4b), $NO_2 \leftrightarrow Al{-}B_4N_{10}$ (Fig.4c), $NO_2 \leftrightarrow Si{-}B_4N_{10}$ (Fig. 4d), $N_2O \leftrightarrow Al{-}B_4N_{10}$ (Fig. 4e), and $N_2O \leftrightarrow Si{-}B_4N_{10}$ (Fig. 4f) denote the fluctuation in the chemical shielding during ion trapping. In fact, Fig. 4 indicates that the gap chemical shielding between aluminum, carbon, silicon doping of $M{-}B_4N_{10}$ nanocage and gas molecules. Therefore, it can be considered that the efficiency of electron accepting for doping atoms on the $M{-}B_4N_{10}$ through gas molecules adsorption can be ordered as: $Si > Al \gg C$ that indicates the power of covalent bond between aluminum, carbon, silicon, and these NO, NO_2, N_2O towards toxic gas removal from air.

In the NMR spectroscopy, it has been observed the remarkable peaks around interaction of NO, NO_2, N_2O molecules through adsorbing on the $M{-}B_4N_{10}$ during toxic gas detection and removal from air; however, there are some fluctuations in the chemical shielding behaviors of isotropic and anisotropy attributes. Therefore, the authors believe that the extracted results would be useful in the design of $M{-}B_4N_{10}$ based doped nanomaterials for increasing the adsorption of gas molecules in addition to the structural studies using solid-state and solution NMR techniques.

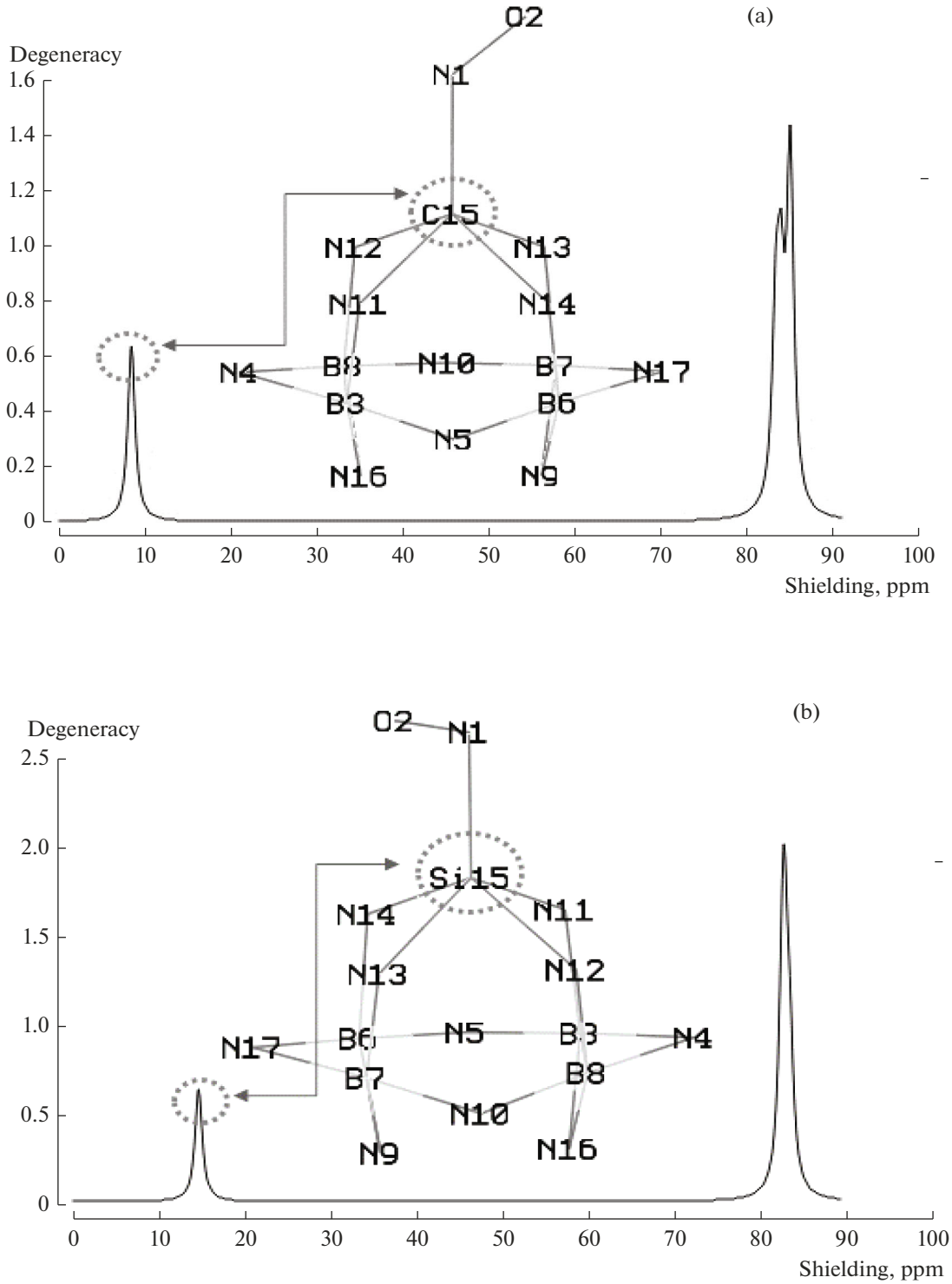

Fig. 4. The NMR spectra for (a) NO ↔ C–B_4N_{10}, (b) NO ↔ Si–B_4N_{10}, (c) NO_2 ↔ Al–B_4N_{10}, (d) NO_2 ↔ Si–B_4N_{10}, (e) N_2O ↔ Al–B_4N_{10} and (f) N_2O ↔ Si–B_4N_{10} complexes using CAM–B3LYP–D3/6-311+G(*d*, *p*), LANL2DZ.

Infrared Spectroscopy and Thermodynamic Factors

The infrared (IR) calculations have been accomplished for adsorption of NO, NO_2, N_2O molecules by M–B_4N_{10} during toxic gas sensing in air. Therefore, it has been simulated the several clusters containing NO ↔ C–B_4N_{10} (Fig. 5a), NO ↔ Si–B_4N_{10} (Fig. 5b), NO_2 ↔ Al–B_4N_{10} (Fig. 5c), NO_2 ↔ Si–B_4N_{10} (Fig. 5d), N_2O ↔ Al–B_4N_{10} (Fig. 5e) and N_2O ↔ C–B_4N_{10} (Fig. 5f) complexes using CAM–B3LYP–D3/6-311+G (d, p), LANL2DZ. The graph of Fig. 5a

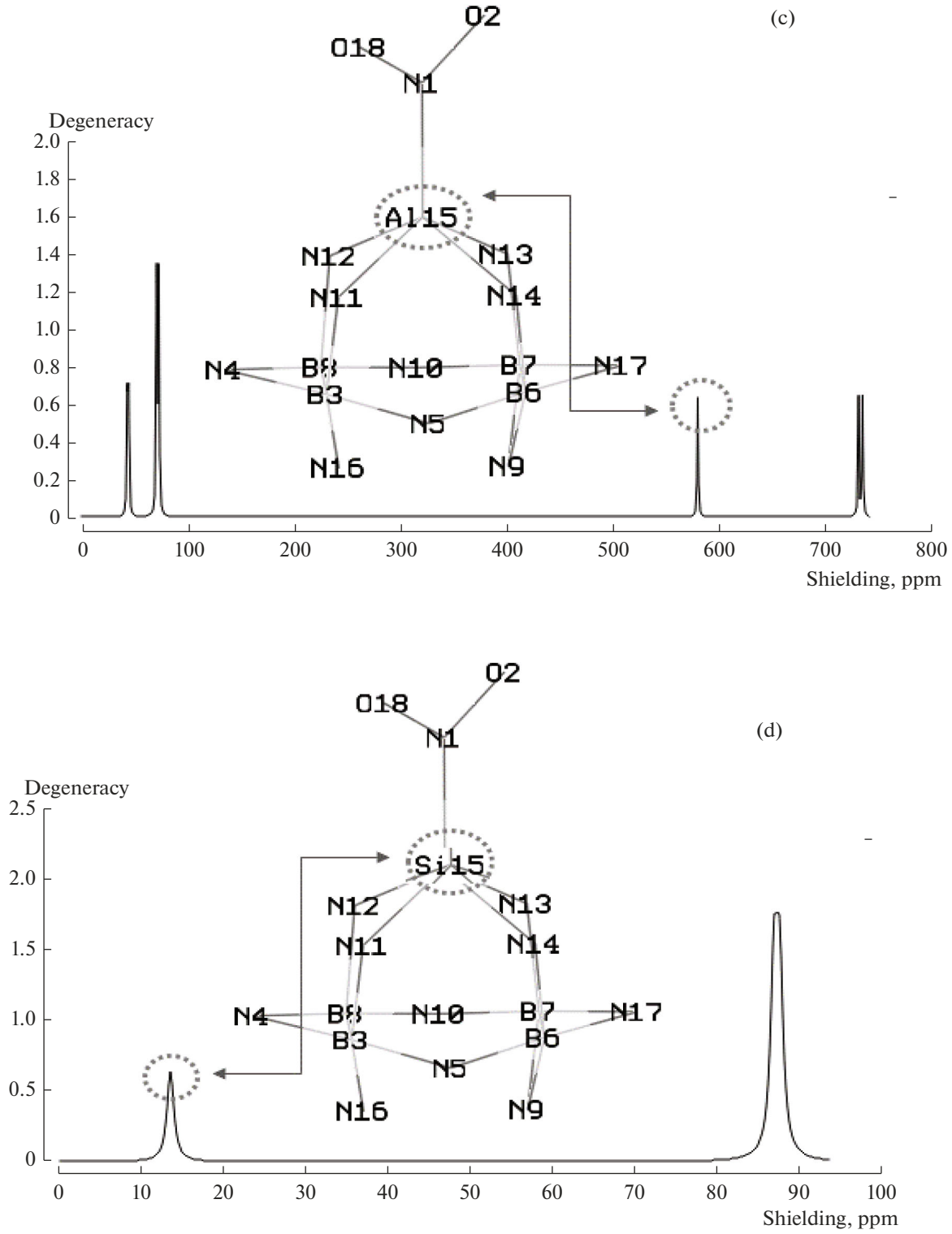

Fig. 4. (Contd.)

has been observed in the frequency range between 200–800 cm^{-1} for NO ↔ C–B_4N_{10} with several sharp peaks around 327.09, 337.61, 359.54, 595.74 and 664.20 cm^{-1}. Figure 5b has shown the frequency range between 200–1100 cm^{-1} for NO ↔ Si–B_4N_{10} with sharp peaks around 652.05, 682.12, 685.59, and

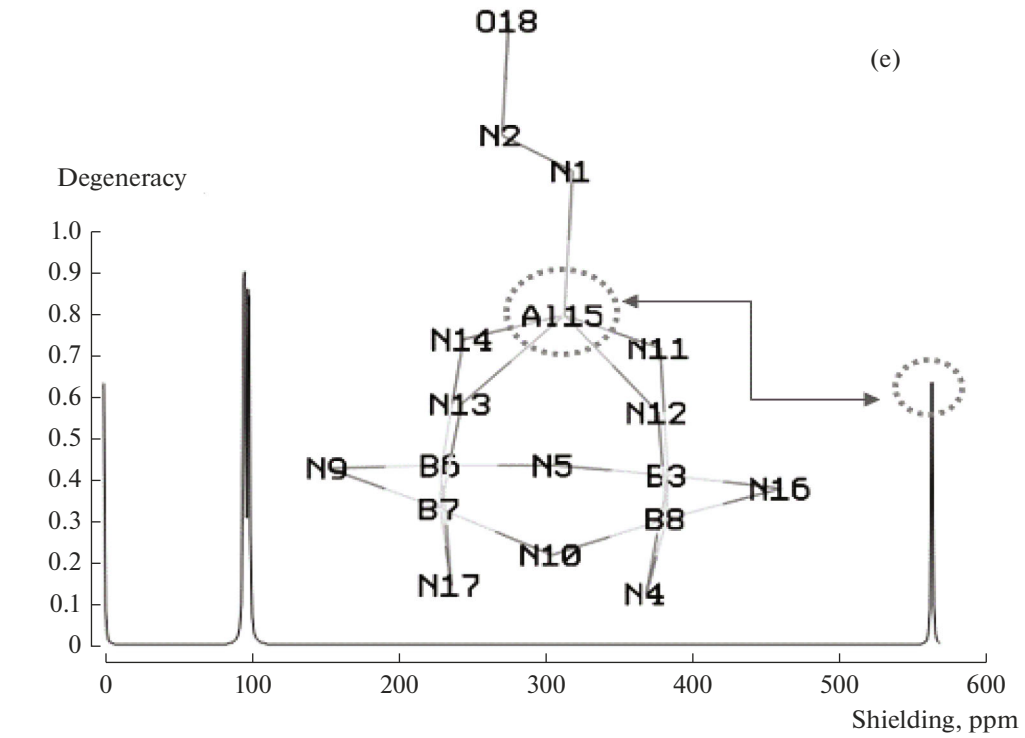
(e)
O18
N2
N1
Degeneracy
1.0
0.9
0.8
0.7
0.6
0.5
0.4
0.3
0.2
0.1
0
Al15
N14
N11
N13
N12
N9
B6
N5
B3
N16
B7
B8
N10
N17
N4
0
100
200
300
400
500
600
Shielding, ppm

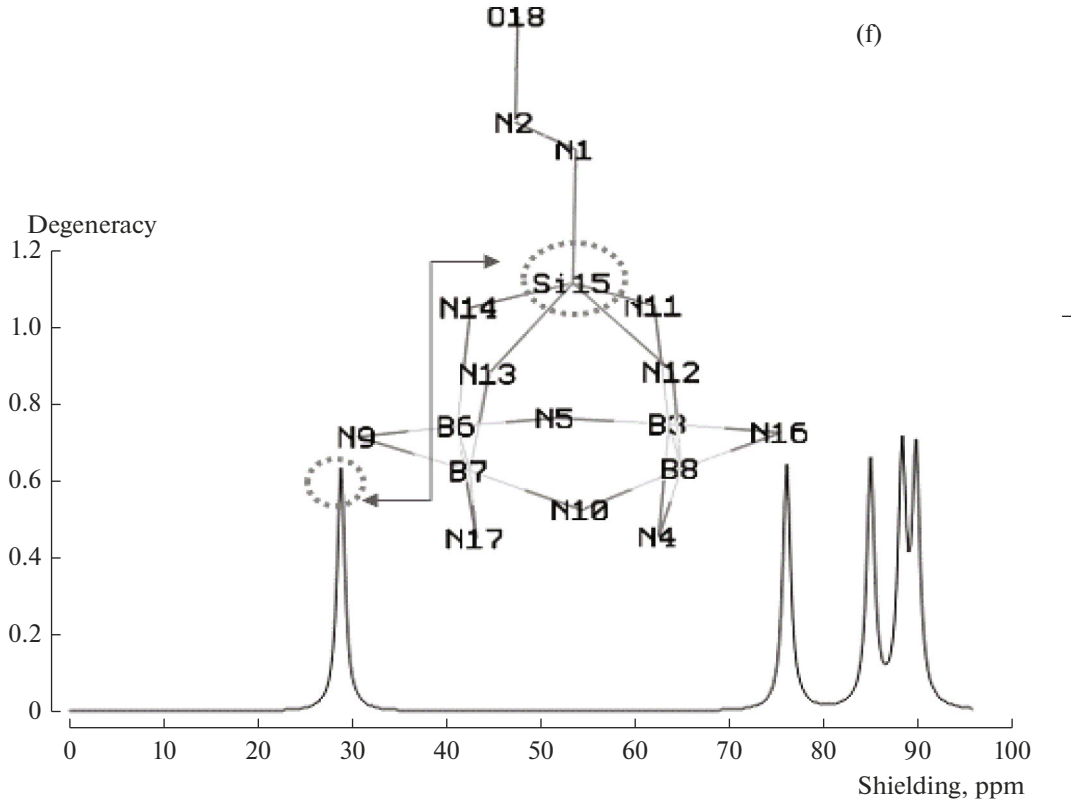
(f)
O18
N2
N1
Degeneracy
1.2
1.0
0.8
0.6
0.4
0.2
0
Si15
N14
N11
N13
N12
N9
B6
N5
B3
N16
B7
B8
N10
N17
N4
0
10
20
30
40
50
60
70
80
90
100
Shielding, ppm

Fig. 4. (Contd.)

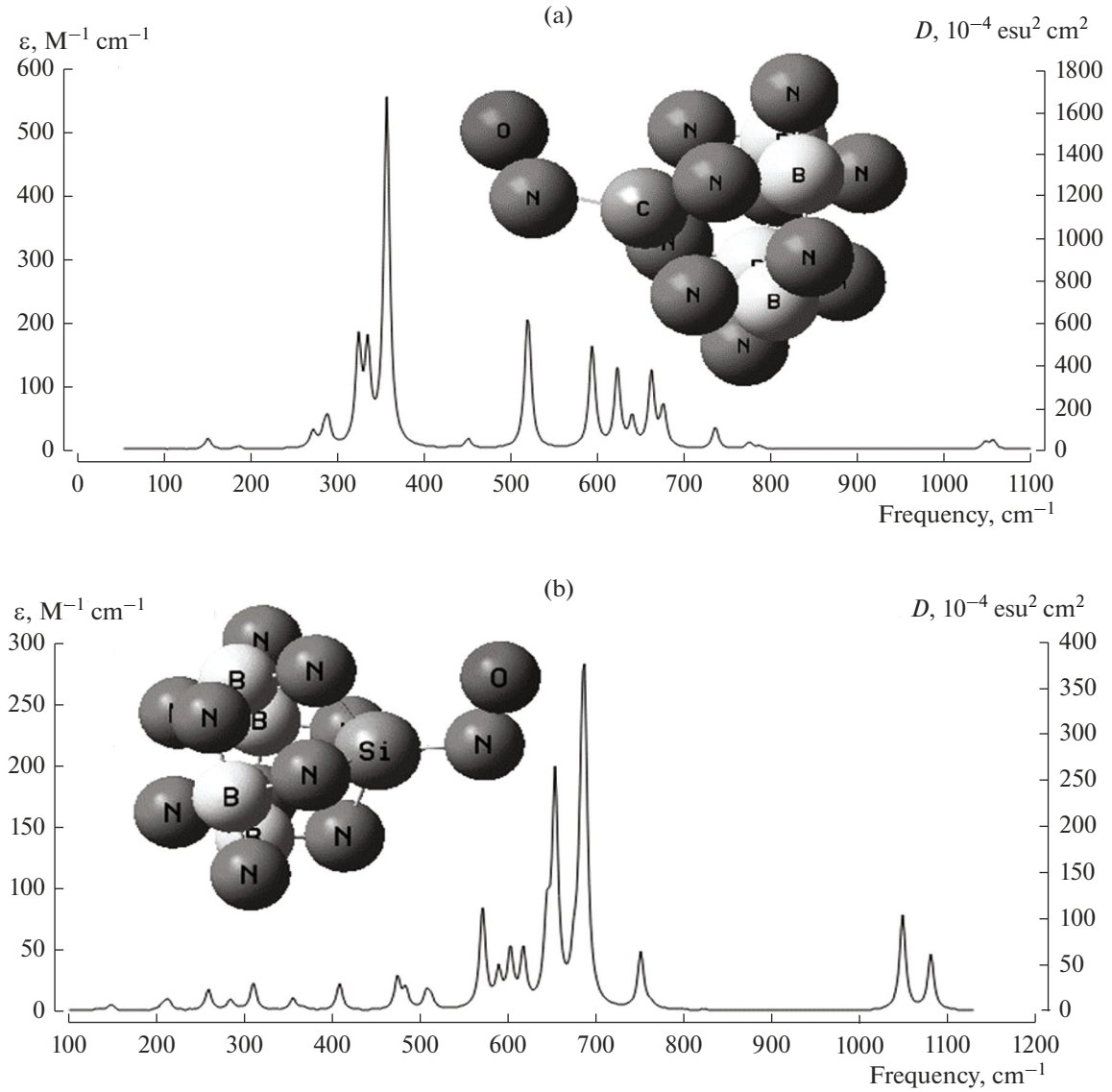

Fig. 5. The Frequency (cm^{-1}) changes through the IR spectra for (a) NO ↔ C–B_4N_{10}, (b) NO ↔ Si–B_4N_{10}, (c) NO_2 ↔ Al–B_4N_{10}, (d) NO_2 ↔ Si–B_4N_{10}, (e) N_2O ↔ Al–B_4N_{10} and (f) N_2O ↔ C–B_4N_{10} complexes using CAM–B3LYP–D3/6-311+G(*d*, *p*), LANL2DZ. [Note: ε (M^{-1} cm^{-1}) is the absorbance unit and *D* (10^{-4} esu^2 cm^2) is the dipole strength via the esu or electrostatic unit, which is a unit of charge in the cgs (centimeter-gram-second system)].

1047.31 cm^{-1}. Figure 5c has indicated the fluctuation of frequency between 100–1100 cm^{-1} for NO_2 ↔ Al–B_4N_{10} with several sharp peaks around 256.25, 335.13, 532.75, and 568.45 cm^{-1}. Figure 5d has shown the fluctuation of frequency between 100–1100 cm^{-1} for NO_2 ↔ Si–B_4N_{10} with a few sharp peaks around 411.31, 451.64, 563.66, 596.34, 685.50, and 758.87 cm^{-1}. Moreover, it has been observed the frequency between 150–900 for N_2O ↔ Al–B_4N_{10} with sharp peaks around 305.94, 315.78, 574.78, 575.58, 717.95, 801.12, 852.32, 863.46, 906.48, 1102.93, and 1126.61 cm^{-1} (Fig. 5e). Besides, Fig. 5f has exhibited the frequency between 100–1200 for N_2O ↔ C–B_4N_{10} with sharp peaks around 345.39, 374.87, 469.76, 528.65, 592.59, 597.92, 624.44, 659.94, 669.69, 702.84, and 706.06 cm^{-1}.

The IR spectra of NO, NO_2, N_2O adsorption with M–B_4N_{10} have demonstrated that the structure of the dominant complex correlates with the electron potency of doped X (Al, C, Si) on the B_5N_{10}. As it has been seen the doped nanocages of C–B_4N_{10} and Si–B_4N_{10} (Figs. 5a and 5b), Al–B_4N_{10} and Si–B_4N_{10} (Figs. 5c and 5d), Al–B_4N_{10} and C–B_4N_{10} (Figs. 5e and 5f), respectively, have the most fluctuations and the highest tendency for adsorption of NO, NO_2 and

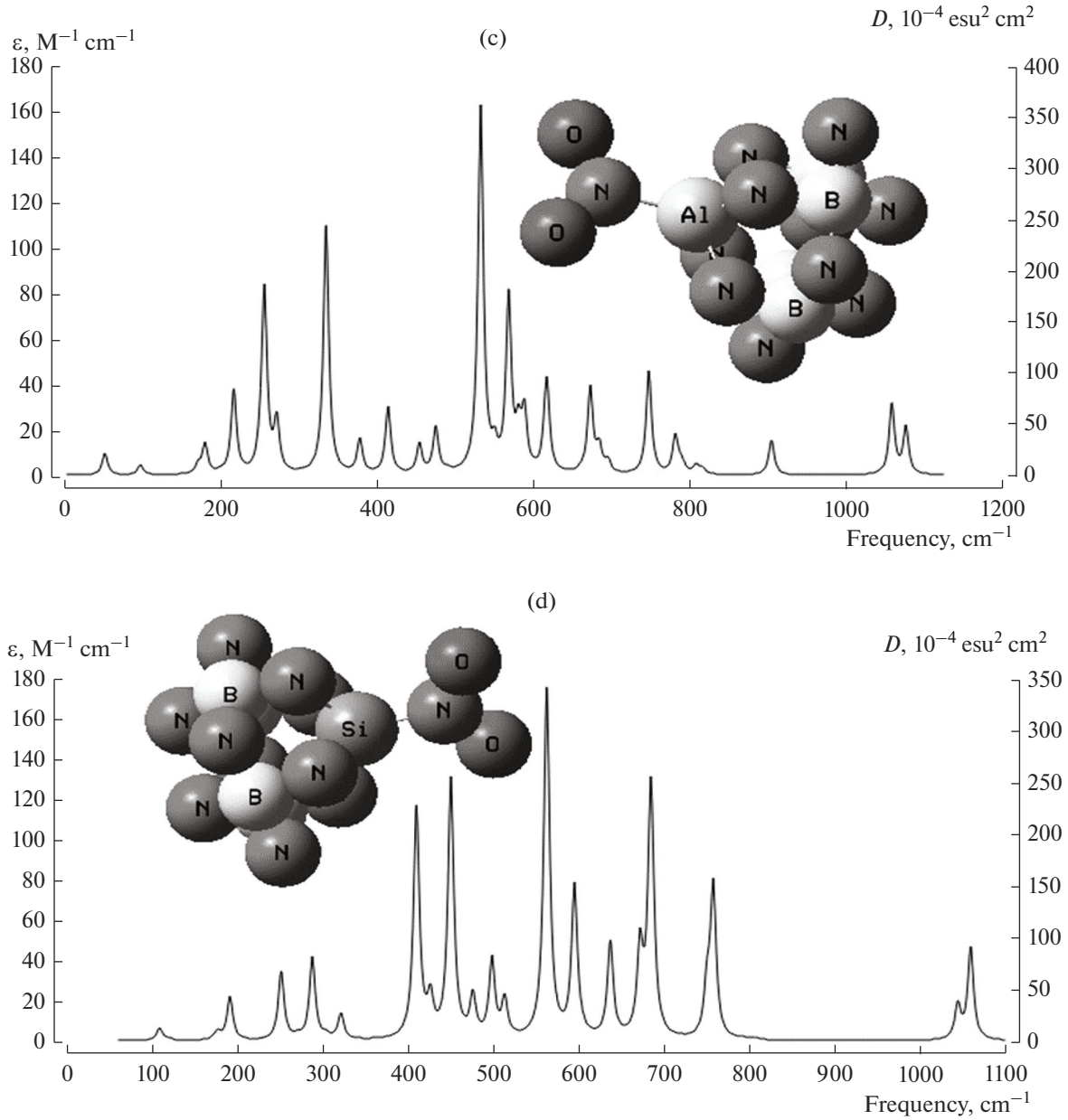

Fig. 5. (Contd.)

N_2O, respectively, (Figs. 5a and 5b). Therefore, it can be found that IR spectroscopy of (G)-adsorbed M–B_4N_{10} is now well-placed to address specific questions on the individual effect of charge carriers (gas molecule-nanocage), as well as doping atoms on the overall structure (Fig. 5).

Table 3 through the thermodynamic specifications concluded that M–B_4N_{10} due to adsorption of NO, NO_2 and N_2O might be more efficient sensors for detecting and removing the gas molecules from polluted air [75]. Thermodynamic parameters of gas molecules adsorption with M–B_4N_{10} have been determined using DFT theoretical technique [76, 77]. It has been shown that for a given number of nitrogen donor sites in NO, NO_2, N_2O, the stabilities of complexes owing to doping atoms of Al, C, Si can be considered as: $N_2O \leftrightarrow Al{-}B_4N_{10} > NO \leftrightarrow Al{-}B_4N_{10} > NO_2 \leftrightarrow C{-}B_4N_{10} > N_2O \leftrightarrow C{-}B_4N_{10} > NO_2 \leftrightarrow Si{-}B_4N_{10} \approx NO_2 \leftrightarrow Al{-}B_4N_{10} > N_2O \leftrightarrow Si{-}B_4N_{10} > NO \leftrightarrow C{-}B_4N_{10} > NO \leftrightarrow Si{-}B_4N_{10}$ (Table 3). The thermodynamic data in Fig. 6 could detect the maximum efficiency of Al, C, Si atoms doping of B_5N_{10} for gas molecules adsorption through ΔG^{o}_{ads} which depends on the covalent bond between NO, NO_2,

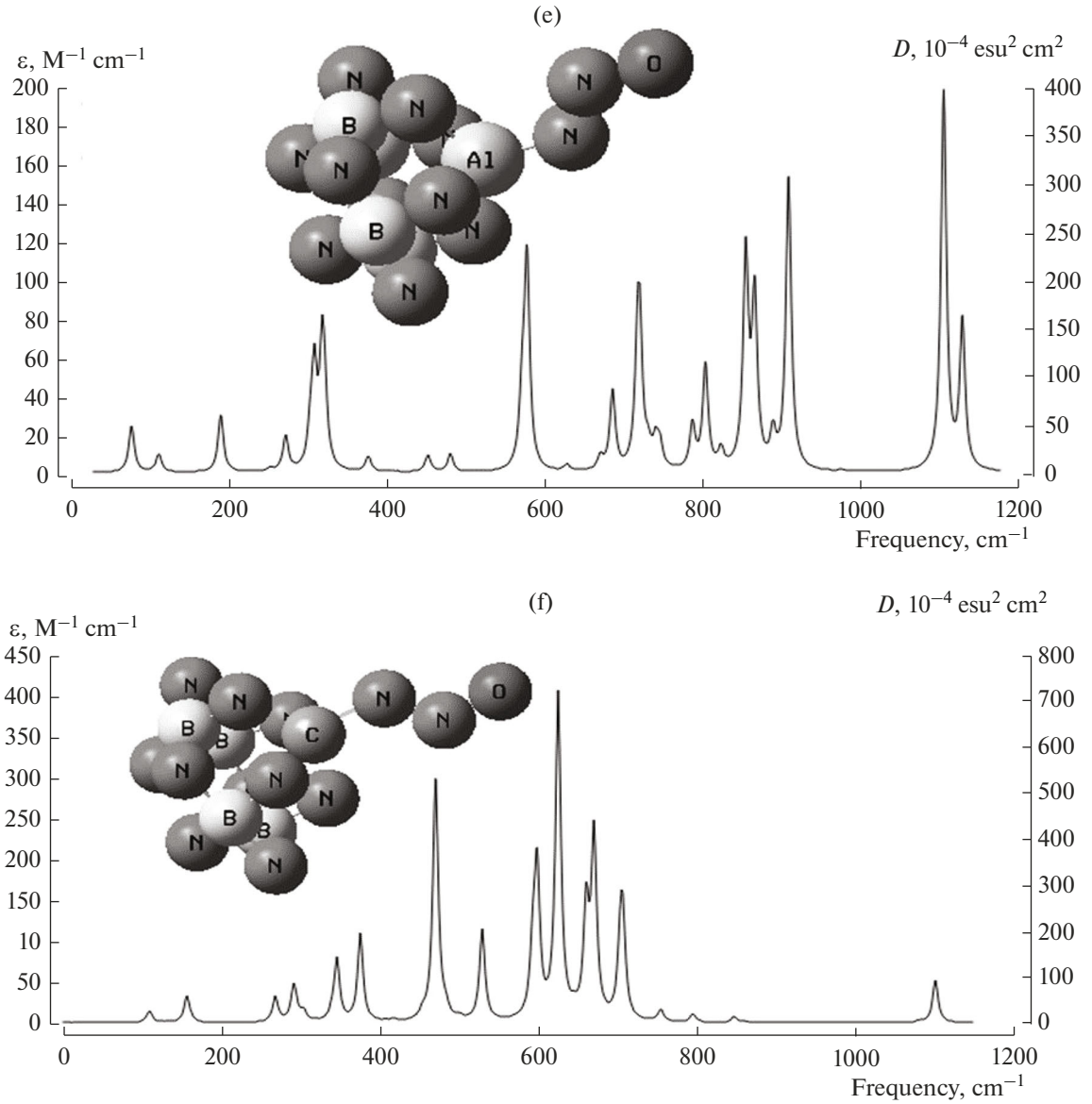

Fig. 5. (Contd.)

Table 3. The thermodynamic characters of NO ↔ Al–B_4N_{10}, NO ↔ C–B_4N_{10}, NO ↔ Si–B_4N_{10}, NO_2 ↔ Al–B_4N_{10}, NO_2 ↔ C–B_4N_{10}, NO_2 ↔ Si–B_4N_{10}, N_2O ↔ Al–B_4N_{10}, N_2O ↔ C–B_4N_{10}, and N_2O↔ Si–B_4N_{10} complexes using CAM–B3LYP–D3/6-311+G(*d*, *p*), LANL2DZ calculation

Compound	Dipole moment, Debye	$\Delta E^o \times 10^{-3}$, kcal/mol	$\Delta H^o \times 10^{-3}$, kcal/mol	$\Delta G^o \times 10^{-3}$, kcal/mol	S^o, cal/K mol
NO ↔ Al–B_4N_{10}	0.60	–631.00	–631.00	–630.92	103.43
NO ↔ C–B_4N_{10}	0.24	–510.55	–510.55	–510.60	103.73
NO ↔ Si–B_4N_{10}	1.13	–489.20	–489.20	–489.24	108.79
NO_2 ↔ Al–B_4N_{10}	5.11	–535.20	–535.20	–535.23	114.34
NO_2 ↔ C–B_4N_{10}	1.43	–557.71	–557.71	–557.74	108.61
NO_2 ↔ Si–B_4N_{10}	2.56	–536.38	–536.37	–536.41	111.93
N_2O ↔ Al–B_4N_{10}	0.70	–664.58	–664.58	–664.61	104.38
N_2O ↔ C–B_4N_{10}	1.97	–544.87	–544.86	–544.90	116.79
N_2O ↔ Si–B_4N_{10}	1.74	–523.52	–523.52	–523.55	114.61

N_2O molecules and $M-B_4N_{10}$ as a potent sensor for air pollution removal.

The adsorption process of NO, NO_2, N_2O molecules on the $M-B_4N_{10}$ is affirmed by the ΔG^o_{ads} quantities:

$$\Delta G^o_{ads} = \Delta G^o_{G\leftrightarrow M-B_4N_{10}} - \left(\Delta G^o_G + \Delta G^o_{M-B_4N_{10}}\right) \quad (4)$$
$$G = NO, NO_2, N_2O \text{ and } M = Al, C, Si.$$

As seen in Table 3, all the accounted ΔG^o_{ads} amounts are very close, which demonstrate the agreement of the measured specifications by all methodologies and the reliability of the computing values. Table 3 has shown that the key role of doped atoms of Al, C, Si during interaction between the adsorbates of NO, NO_2, N_2O molecules as the electron donors and the adsorbent of $Al-B_4N_{10}$, $C-B_4N_{10}$, and $Si-B_4N_{10}$ as electron acceptors. Therefore, the selectivity of atom-doped on boron nitride nanocage (gas sensor) for gas molecules adsorption can be resulted as: Al > C > Si (Table 3).

CONCLUSIONS

This research work has investigated doping of Al, C, Si elements on the boron nitride nanocage ($M-B_4N_{10}$) for enhancing toxic gas sensing of these nanomaterials for air pollution removal. Therefore, NO, NO_2, N_2O molecules separation involving the $M-B_4N_{10}$ has been experimented based on electrostatic interactions between the gas molecules and $M-B_4N_{10}$. The electromagnetic and thermodynamic properties of $M-B_4N_{10}$ complexes were computed using density functional theory. The results have illustrated that chosen gas molecules adsorbed on the $M-B_4N_{10}$ are rather stable with the most stable adsorption site being in the center of $M-B_4N_{10}$ system. The selectivity of atom-doped on boron nitride nanocage (gas sensor) for gas molecules adsorption can be resulted as: $C-B_4N_{10}$ and $Si-B_4N_{10}$ for NO, $Al-B_4N_{10}$ and $Si-B_4N_{10}$ for NO_2, $Al-B_4N_{10}$ and $C-B_4N_{10}$ for N_2O, respectively. This work proposes that metallic, nonmetallic, metalloid as a semiconductor can be examined through doping on the nanomaterials for enhancing the adsorption potency towards designing the pollution removal sensors.

ACKNOWLEDGMENTS

In successfully completing this paper and its research, the authors are grateful to Kastamonu University.

FUNDING

This work was supported by ongoing institutional funding. No additional grants to carry out or direct this particular research were obtained.

CONFLICT OF INTEREST

The authors of this work declare that they have no conflicts of interest.

REFERENCES

1. D. Gonzalez-Ortiz, C. Salameh, M. Bechelany, et al., Mater. Today Adv. **8**, 100107 (2020). https://doi.org/10.1016/j.mtadv.2020.100107
2. N. S. Mishra and P. Saravanan, ChemistrySelect **3** (28), 8023–8034 (2018). https://doi.org/10.1002/slct.201801524
3. Q. H. Weng, X. B. Wang, X. Wang, et al., Chem. Soc. Rev. **45** (14), 3989–4012 (2016). https://doi.org/10.1039/C5CS00869G
4. E. C. Anota, SN Appl. Sci. **4**, 295 (2022). https://doi.org/10.1007/s42452-022-05180-z
5. G. V. Simbirtseva and S. D. Babenko, Russ. J. Phys. Chem. B **17**, 1309–1310 (2023). https://doi.org/10.1134/S1990793123060222
6. S. Z. Rogovina, M. M. Gasymov, S. M. Lomakin, et al., Russ. J. Phys. Chem. B **17**, 1376–1383 (2023). https://doi.org/10.1134/S1990793123060088
7. I. A. Palamarchuk, N. A. Gorshkova, O. S. Brovko, et al., Russ. J. Phys. Chem. B **17**, 1434–1441 (2023). https://doi.org/10.1134/S1990793123070096
8. E. I. Rudenko, N. V. Dohlikova, A. K. Gatin, et al., Russ. J. Phys. Chem. B **17**, 845–852 (2023). https://doi.org/10.1134/S1990793123040164
9. D. Zhang, M. Ding, Y. Xu, et al., Russ. J. Phys. Chem. B **17**, 489–494 (2023). https://doi.org/10.1134/S1990793123020331
10. G. V. Simbirtseva, S. D. Babenko, D. P. Kiryukhin, et al., Russ. J. Phys. Chem. B **17**, 107–112 (2023). https://doi.org/10.1134/S1990793123010116
11. V. B. Merinov and V. A. Domnin, Russ. J. Phys. Chem. B **17**, 215–221 (2023). https://doi.org/10.1134/S1990793123010268
12. D. V. Shtansky, A. T. Matveev, E. S. Permyakova, et al., Nanomaterials **12**, 2810 (2022). https://doi.org/10.3390/nano12162810
13. Y. Yang, Y. Peng, M. F. Saleem, et al., Materials **15**, 4396 (2022). https://doi.org/10.3390/ma15134396
14. A. Davies, J. D. Albar, A. Summerfield, et al., Nano Lett. **18**, 498–504 (2018). https://doi.org/10.1021/acs.nanolett.7b04453
15. F. Mollaamin, S. Mohammadi, Z. Khalaj, et al., Russ. J. Phys. Chem. B **18** (1), 67–82 (2024). https://doi.org/10.1134/S1990793124010330
16. R. S. Bangari, V. K. Yadav, J. K. Singh, et al., ACS Omega **5**, 10301–10314 (2020). https://doi.org/10.1021/acsomega.9b04295
17. Y. H. Chao, J. Zhang, H. P. Li, et al., Chem. Eng. J. **387**, 124138 (2020). https://doi.org/10.1016/j.cej.2020.124138
18. Y. Guo, R. X. Wang, P. F. Wang, et al., ACS Sustain. Chem. **7**, 5727–5741 (2019). https://doi.org/10.1021/ACSSUSCHEMENG.8B05150

19. A. A. Eganov, D. A. Kardonsky, I. V. Sulimenkov, et al., Russ. J. Phys. Chem. B **17**, 503–509 (2023). https://doi.org/10.1134/S1990793123020240
20. M. Monajjemi, M. Khaleghian, N. Tadayonpour, et al., Int. J. Nanosci. **09**, 517–529 (2010). https://doi.org/10.1142/S0219581X10007071
21. M. Monajjemi, V. S. Lee, M. Khaleghian, et al., J. Phys. Chem. C **114**, 15315 (2010). https://doi.org/10.1021/jp104274z
22. F. Mollaamin and M. Monajjemi, Sensor Rev. **43**, 266–279 (2023). https://doi.org/10.1108/SR-03-2023-0040
23. S. Shahriari, F. Mollaamin, and M. Monajjemi, Micromachines **14**, 241 (2023). https://doi.org/10.3390/mi14020241
24. F. Mollaamin and M. Monajjemi, J. Mol. Model. **29**, 170 (2023). https://doi.org/10.1007/s00894-023-05567-8
25. F. Mollaamin, S. Shahriari, M. Monajjemi, et al., J. Clust. Sci. **34**, 1547–1562 (2023). https://doi.org/10.1007/s10876-022-02335-1
26. F. Mollaamin, M. Monajjemi, S. Salemi, et al., Fullerenes, Nanotubes Carbon Nanostruct. **19**, 182 (2011). https://doi.org/10.1080/15363831003782932
27. A. Tahan, F. Mollaamin, and M. Monajjemi, Russ. J. Phys. Chem. **83**, 587–597 (2009). https://doi.org/10.1134/S003602440904013X
28. G. Henkelman, A. Arnaldsson, and H. Jónsson, Comput. Mater. Sci. **36** (3), 354–360 (2006). https://doi.org/10.1016/j.commatsci.2005.04.010
29. F. Mollaamin and M. Monajjemi, Sensor Rev. **44** (2), 179–193 (2024). https://doi.org/10.1108/SR-01-2024-0066
30. E. M. Sarasia, S. Afsharnezhad, B. Honarparvar, et al., Phys. Chem. Liq. **49**, 561–571 (2011). https://doi.org/10.1080/00319101003698992
31. M. Khaleghian, M. Zahmatkesh, F. Mollaamin, et al., Fullerenes, Nanotubes Carbon Nanostruct. **19**, 251–261 (2011). https://doi.org/10.1080/15363831003721757
32. M. Monajjemi, F. Mollaamin, and S. Shojaei, Biointerface Res. Appl. Chem. **10**, 5575 (2020). https://doi.org/10.33263/BRIAC103.575585
33. S. Shahriari, M. Monajjemi, and F. Mollaamin, J. Chil. Chem. Soc. **67**, 5468–5476 (2022). https://doi.org/10.4067/S0717-97072022000205468
34. F. Mollaamin and M. Monajjemi, Sensor Rev. **44** (2), 100–112. https://doi.org/10.1108/SR-05-2023-0148
35. X. Miao, S. Zhou, and C. Wang, Russ. J. Phys. Chem. B **16**, 804–808 (2022). https://doi.org/10.1134/S199079312204011X
36. M. Monajjemi, L. Mahdavian, F. Mollaamin, et al., Russ. J. Inorg. Chem. **54**, 1465–1473 (2009). https://doi.org/10.1134/S0036023609090216
37. F Mollaamin and M. Monajjemi, J. Comput. Theor. Nanosci. **12**, 1030–1039 (2015). https://doi.org/10.1166/jctn.2015.3846
38. F. Mollaamin, A. Ilkhani, N. Sakhaei, et al., J. Comput. Theor. Nanosci. **12**, 3148–3154 (2015). https://doi.org/10.1166/jctn.2015.4092
39. F. Mollaamin and M. Monajjemi, J. Mol. Struct. **1300**, 137214 (2024). https://doi.org/10.1016/j.molstruc.2023.137214
40. M. Monajjemi, S. Mohammadi, S. Shahriari, et al. Russ. J. Phys. Chem. B **18**, 308–324 (2024). https://doi.org/10.1134/S1990793124010342
41. J. P. Perdew, K. Burke and M. Ernzerhof, Phys. Rev. Lett. **77**, 3865 (1996). https://doi.org/10.1103/PhysRevLett.77.3865
42. F. Mollaamin, S. Shahriari, M. Monajjemi, et al., J. Cluster Sci. **34**, 1547–1562 (2023). https://doi.org/10.1007/s10876-022-02335-1
43. M. Monajjemi, F. Mollaamin, and S. Shojaei, Biointerface Res. Appl. Chem. **10**, 5575 (2020). https://doi.org/10.33263/BRIAC103.575585
44. F. Mollaamin and M. Monajjemi, Mol. Simul. **49**, 365 (2023). https://doi.org/10.1080/08927022.2022.2159996
45. M. A. A. Zadeh, H. Lari, L. Kharghanian, et al., J. Comput. Theor. Nanosci. **12**, 4358 (2015). https://doi.org/10.1166/jctn.2015.4366
46. F. Mollaamin and M. Monajjemi, Russ. J. Phys. Chem. B **18**, 533–548 (2024). https://doi.org/10.1134/S199079312402012X
47. P. Ziesche, S. Kurth, J.P. Perdew, Comput. Mater. Sci. **11**, 122–127 (1998). https://doi.org/10.1016/S0927-0256(97)00206-1
48. M. Arrigoni and G. K. H. Madsen, Comput. Mater. Sci. **156**, 354–360 (2019). https://doi.org/10.1016/j.commatsci.2018.10.005
49. P. Hohenberg and W. Kohn, Phys. Rev. B **136**, B864–B871 (1964). https://doi.org/10.1103/PhysRev.136.B864
50. W. Kohn and L. J. Sham, Phys. Rev. **140**, A1133–A1138 (1965). https://doi.org/10.1103/PhysRev.140.A1133
51. H. Touhami, K. Almi, S.Lakel, et al., Russ. J. Phys. Chem. B **17**, 1057–1068 (2023). https://doi.org/10.1134/S1990793123050287
52. A. D. Becke, J. Chem. Phys. **98**, 5648–5652 (1993). https://doi.org/10.1063/1.464913
53. C. Lee, W. Yang, and R. G. Parr, Phys. Rev. B **37**, 785–789 (1988). https://doi.org/10.1103/PhysRevB.37.785
54. G. M. Khrapkovskii, I. V. Aristov, D. L. Egorov, et al., Russ. J. Phys. Chem. B **16**, 862–868 (2022). https://doi.org/10.1134/S1990793122040066
55. C. J. Cramer, *Essentials of Computational Chemistry: Theories and Models*, 2nd ed. (Wiley, 2004).
56. F. Mollaamin and M. Monajjemi, Russ. J. Phys. Chem. B **18**, 49–66 (2024). https://doi.org/10.1134/S1990793124010159
57. K. Bakhshi, F. Mollaamin and M. Monajjemi, J. Comput. Theor. Nanosci. **8**, 763–768 (2011). https://doi.org/10.1166/jctn.2011.1750
58. F. Mollaamin and M. Monajjemi, Russ. J. Phys. Chem. B **17** (3), 658–672 (2023). https://doi.org/10.1134/s1990793123030223

59. F. Mollaamin and M. Monajjemi, Russ. J. Phys. Chem. B **18** (2), 607–623 (2024). https://doi.org/10.1134/S1990793124020271

60. F. Mollaamin and M. Monajjemi, J. Mol. Model. **29**, 119 (2023). https://doi.org/10.1007/s00894-023-05526-3

61. M. Monajjemi, M. T. Baie, and F. Mollaamin, Russ. Chem. Bull. **59**, 886–889 (2010). https://doi.org/10.1007/s11172-010-0181-5

62. M. J. Frisch, G. W. Trucks, H. B. Schlegel, G. E. Scuseria, M. A. Robb, J. R. Cheeseman, G. Scalmani, V. Barone, G. A. Petersson, H. Nakatsuji, X. Li, M. Caricato, A. V. Marenich, J. Bloino, B. G. Janesko, R. Gomperts, B. Mennucci, H. P. Hratchian, J. V. Orti|z, A. F. Izmaylov, J. L. Sonnenberg, D. Williams-Young, F. Ding, F. Lipparini, F. Egidi, J. Goings, B. Peng, A. Petrone, T. Henderson, D. Ranasinghe, V. G. Zakrzewski, J. Gao, N. Rega, G. Zheng, W. Liang, M. Hada, M. Ehara, K. Toyota, R. Fukuda, J. Hasegawa, M. Ishida, T. Nakajima, Y. Honda, O. Kitao, H. Nakai, T. Vreven, K. Throssell, J. A. Montgomery, Jr., J. E. Peralta, F. Ogliaro, M. J. Bearpark, J. J. Heyd, E. N. Brothers, K. N. Kudin, V. N. Staroverov, T. A. Keith, R. Kobayashi, J. Normand, K. Raghavachari, A. P. Rendell, J. C. Burant, S. S. Iyengar, J. Tomasi, M. Cossi, J. M. Millam, M. Klene, C. Adamo, R. Cammi, J. W. Ochterski, R. L. Martin, K. Morokuma, O. Farkas, J. B. Foresman, and D. J. Fox, Gaussian 16, Revision C.01 (Gaussian, Inc., Wallingford CT, 2016).

63. R. Dennington, T. A. Keith, and J. M. Millam, GaussView, Version 6.06.16 (Semichem Inc., Shawnee Mission, KS, 2016).

64. L. I. Trakhtenberg, Russ. J. Phys. Chem. B **17**, 600–607 (2023). https://doi.org/10.1134/S1990793123030144

65. I. S. Golyak, D. R. Anfimov, I. B. Vintaykin, et al., Russ. J. Phys. Chem. B **17**, 320–328 (2023). https://doi.org/10.1134/S1990793123020264

66. J. Smith, Nature **270**, 663 (1977). https://doi.org/10.1038/270663a0

67. S. N. Kozlov and B. E. Zhestkov, Russ. J. Phys. Chem. B **16**, 1030–1037 (2022). https://doi.org/10.1134/S1990793122060069

68. T. A. Ivanova, E. M. Zubanova, A. A. Popova, et al., Russ. J. Phys. Chem. B **16**, 1208–1212 (2022). https://doi.org/10.1134/S1990793122070089

69. V. V. Zelenov and E. V. Aparina, Russ. J. Phys. Chem. B **16**, 1182–1190 (2022). https://doi.org/10.1134/S1990793122060239

70. U. Sohail, F. Ullah, N. H. Binti Zainal Arfan, et al., Molecules **28**, 4060 (2023). https://doi.org/10.3390/molecules28104060

71. F. Mollaamin and M. Monajjemi, Sensor Rev. **43**, 266–279 (2023). https://doi.org/10.1108/SR-03-2023-0040

72. B. Khalili Hadad, F. Mollaamin, and M. Monajjemi, Russ. Chem. Bull. **60**, 238–241 (2011). https://doi.org/10.1007/s11172-011-0039-5

73. F. Mollaamin and M. Monajjemi, J. Cluster Sci. **34**, 2901–2018 (2023). https://doi.org/10.1007/s10876-023-02436-5

74. F. Mollaamin and M. Monajjemi, Int. J. Quantum Chem. **124**, e27348 (2024). https://doi.org/10.1002/qua.27348

75. M. M. Avilova, N. V. Zolotareva, and O. V. Popova, Russ. J. Phys. Chem. B **17**, 329–335 (2023). https://doi.org/10.1134/S1990793123020203

76. E. M. Zubanova, D. A. Rubtsov, and E. N. Golubeva, Russ. J. Phys. Chem. B **17**, 790–795 (2023). https://doi.org/10.1134/S199079312304019X

77. N. A. Kochetov and B. S. Seplyarskii, Russ. J. Phys. Chem. B **17**, 381–387 (2023). https://doi.org/10.1134/S1990793123020082